BAMS Article

CAIPEEX

Indian Cloud Seeding Scientific Experiment

Thara Prabhakaran, P. Murugavel, Mahen Konwar, Neelam Malap, K. Gayatri, Shivsai Dixit, Soumya Samanta, Subharthi Chowdhuri, Sudarsan Bera, Mercy Varghese, J. Rao, J. Sandeep, P. D. Safai, A. K. Sahai, Duncan Axisa, A. Karipot, Darrel Baumgardner, Benjamin Werden, Ed Fortner, Kurt Hibert, Sathy Nair, Shivdas Bankar, Dinesh Gurnule, Kiran Todekar, Jerry Jose, V. Jayachandran, Pawan S. Soyam, Abhishek Gupta, Harish Choudhary, Aravindhavel, Suresh Babu Kantipudi, P. Pradeepkumar, R. Krishnan, K. Nandakumar, Peter F. DeCarlo, Doug Worsnop, G. S. Bhat, M. Rajeevan, and Ravi Nanjundiah

KEYWORDS:
Aerosols;
Cloud droplets;
Clouds;
Cumulus clouds;
Drop size distribution;
Cloud seeding

ABSTRACT: The demand for effective methods to augment precipitation over arid regions of India has been increasing over the past several decades as the changing climate brings warmer average temperatures. In the fourth phase of the Cloud Aerosol Interaction and Precipitation Enhancement Experiment (CAIPEEX IV), a scientific investigation was conducted over a rain-shadow region of the Western Ghats mountains in India. The primary objective was to investigate the efficacy of hygroscopic seeding in convective clouds and to develop a cloud seeding protocol. CAIPEEX IV followed the World Meteorological Organization (WMO) recommendations in a peer-reviewed report with physical, statistical, and numerical investigations. The initial results of the campaign in the monsoon period of 2018 and 2019 with two instrumented aircraft, a ground-based dual-polarization C-band radar, a network of rain gauges, radiosondes, and surface aerosol measurements are reported here. The hygroscopic seeding material was detected in cloud droplets and key cloud microphysical processes in the seeding hypothesis were tracked. The formidable challenges of assessing seeding impacts in convective clouds and the results from 150 seed and 122 no-seed samples of randomized experiments are illustrated. Over 5,000 cloud passes from the airborne campaign provided details about the convective cloud properties as the key indicators for a seeding strategy and the evaluation protocol. The experimental results suggest that cloud seeding can be approached scientifically to reduce uncertainty. The results from this study should interest the scientific community and policymakers concerned with climate change's impact on precipitation and how to mitigate rainfall deficiencies.

https://doi.org/10.1175/BAMS-D-21-0291.1
Corresponding author: Thara Prabhakaran, thara@tropmet.res.in
Supplemental material: https://doi.org/10.1175/BAMS-D-21-0291.2
In final form 6 October 2023

AFFILIATIONS: Prabhakaran, Murugavel, Konwar, Malap, Gayatri, Dixit, Samanta, Bera, Varghese, Rao, Sandeep, Safai, Sahai, Nair, Bankar, Gurnule, Todekar, Jayachandran, Soyam, Gupta, Choudhary, Aravindhavel, Kantipudi, and Krishnan—Indian Institute of Tropical Meteorology, Ministry of Earth Sciences, Pune, India; **Chowdhuri**—Indian Institute of Tropical Meteorology, Ministry of Earth Sciences, Pune, India, and Department of Civil and Environmental Engineering, University of California, Irvine, Irvine, California; **Axisa**—Center for Western Weather and Water Extremes, Scripps Institute of Oceanography, La Jolla, California; **Karipot and Pradeepkumar**—Department of Atmospheric and Space Sciences, Savitribai Phule Pune University, Pune, India; **Baumgardner**—Droplet Measurement Technologies, LLC, Longmont, Colorado; **Werden, Fortner, and Worsnop**—Aerodyne Research Inc., Billerica, Massachusetts; **Hibert**—Weather Modification Inc., Fargo, North Dakota; **Jose and Nandakumar**—Mahatma Gandhi University, Athirampuzha, India; **DeCarlo**—The Johns Hopkins University, Baltimore, Maryland; **Bhat**—Centre for Atmospheric and Oceanic Sciences, Indian Institute of Science, Bengaluru, India; **Rajeevan**—National Centre for Earth Science Studies, Ministry of Earth Sciences, Akkulam, India; **Nanjundiah**—Indian Institute of Tropical Meteorology, Ministry of Earth Sciences, Pune, and Centre for Atmospheric and Oceanic Sciences, Indian Institute of Science, Bengaluru, India

Monsoon rains are the lifeline of millions of people, during which seasonal southwesterly winds bring moisture over the Indian subcontinent. The moisture-laden monsoon winds coming from the Arabian Sea are orographically lifted over the Western Ghats (WG) in the Indian peninsular region (Sarker 1966; Houze 2012) and forced to condense and precipitate on the windward side of the WG (Konwar et al. 2014). The annual rainfall over the leeward side is only 10% (600 mm) of the total rainfall received on the windward slopes of the WG. As a result, the leeward side is semiarid and frequently subject to severe drought conditions (Takle and Pai 2020). Prolonged droughts due to global warming and climate change (Krishnan et al. 2020) could introduce additional stress for areas already suffering from water scarcity. Therefore, local and governmental agencies seek viable mitigation solutions to these problems. Previously, several state governments have carried out operational cloud seeding in this region (Nagaraja and Manikiam 2020; Kulkarni et al. 2019); however, a scientific basis for such activities was lacking. To address this, the Indian government initiated a multiyear Cloud–Aerosol Interaction and Precipitation Enhancement Experiment (CAIPEEX; Prabha et al. 2011; Kulkarni et al. 2012), implemented by the Indian Institute of Tropical Meteorology (IITM).

CAIPEEX was planned with two primary objectives, namely, 1) to document in situ aerosol and cloud microphysical properties over India throughout the monsoon season to understand aerosol–cloud–precipitation interactions and 2) to conduct randomization experiments for determining the efficacy of hygroscopic seeding. Here, we first provide a historical perspective of hygroscopic cloud seeding to put the CAIPEEX studies into context. The CAIPEEX program is then described, which includes details of the ground-based and airborne measurements, the strategy for hygroscopic seeding and seed particle tracking within clouds, the physical and randomization experiments, and finally, a glimpse of numerical modeling results.

Historical perspective

The World Meteorological Organization (WMO) issued an expert report that reviewed the current state of cloud seeding science and concluded that one of the major challenges is to reduce the uncertainty in quantifying the effects of cloud seeding used to enhance precipitation

(Flossmann et al. 2018). Another peer-reviewed publication discussed the research programs needed to provide scientific evidence of the efficacy of cloud seeding to produce the desired effect (Flossmann et al. 2019). In particular, the evidence supporting rain enhancement from seeding should be reproducible and follow rigorous statistical and physical evaluations supported by numerical simulations. Numerous seeding trials are needed that include a variety of environmental and background aerosol conditions akin to the target area and documentation that demonstrates the repeatable nature of the outcome of seeding. The size and composition of aerosol particles determine cloud properties (Albrecht 1989; Andreae et al. 2004; Rosenfeld et al. 2008, and references therein).

Hygroscopic seeding, where convective clouds are seeded at their warm cloud bases with seed particles that activate as water droplets at low supersaturation, has enumerable challenges. These include the complex dynamic processes associated with convective clouds, a wide range of ambient cloud condensation nuclei (CCN) concentrations, land use and boundary layer interactions, and orographic features, all impacting cloud formation and evolution. The introduction of seed particles, more hygroscopic compared to the background aerosol, is designed to broaden the cloud droplet size distribution near the cloud base, leading to coalescence that forms drizzle and raindrops earlier in the development of the cloud than would have occurred naturally. The hygroscopic seeding experiment in Queensland, Australia (Tessendorf et al. 2012, 2021), the United Arab Emirates (UAE) Research Program for Rain Enhancement Science (UAEREP), and other efforts discussed by Flossmann et al. (2019) all have strong research components (a more exhaustive list is provided in Supplement A). These projects laid the foundation for the design and implementation of CAIPEEX, whose underlying hypotheses are similar to those described by Flossmann et al. (2019). To evaluate the seeding hypotheses, the physical chain of events in the precipitation process must be documented with advanced observational technologies to characterize cloud properties (Tessendorf et al. 2012) and supported by seeding models like in the glaciogenic seeding experiments (Xue et al. 2013, 2014, 2016, 2017, 2022).

Motivation: Indian scenario and CAIPEEX

Driven by the ever-increasing demand for water and the need to evaluate the efficacy of cloud seeding, the Indian Institute of Tropical Meteorology (IITM) conducted several cloud seeding experiments previously over the Baramati region in Maharashtra (Murty et al. 2000, and references therein). Since warm clouds dominate the region, salt (NaCl) was used as seeding material and was dispersed over an area without targeting isolated clouds. Estimates indicated a 24% increase in precipitation (Murty et al. 2000) with airborne hygroscopic seeding. Modern observational techniques were not available then for process-level evaluations, and therefore, the inferences regarding seeding efficacy were not robust. Several other states carried out operational cloud seeding (Kulkarni et al. 2019) when drought-like situations arose. These operational seeding projects aimed to mitigate drought but lacked detailed scientific investigation and quantification of the seeding efficacy.

Considering the repeated demand for operational cloud seeding from different states on the one hand and the associated cost and uncertainties involved on the other, the CAIPEEX program for the scientific evaluation of cloud seeding was initiated. The core objective of CAIPEEX is to carry out advanced research on aerosol–cloud–precipitation interactions over the Indian subcontinent and to formulate a scientific basis for rain enhancement options. CAIPEEX started in 2009 and was executed in four phases. The fourth phase was focused on the cloud seeding experiment to assess the efficiency of hygroscopic cloud seeding.

Phase IV, carried out in 2018 and 2019, focused on the scientific evaluation of cloud seeding based on previous research (see Supplement A) and as per the WMO (2015, 2018)

recommendations. Two types of field experiments are conducted: randomization experiments aimed at robustly estimating the efficacy of cloud seeding statistically and physical experiments designed to gain not only a deeper understanding of the processes involved in cloud–aerosol interaction in general and rain enhancement in particular but also to generate a database of high-quality measurements. The observational campaign included three components: 1) airborne observations with two aircraft, one for research and the other for seeding (Fig. 1a); 2) a dense rain gauge network (Fig. 1d); and 3) a ground-based aerosol laboratory, meteorological tower, and radar (Fig. 1e). Seeding signatures were documented using

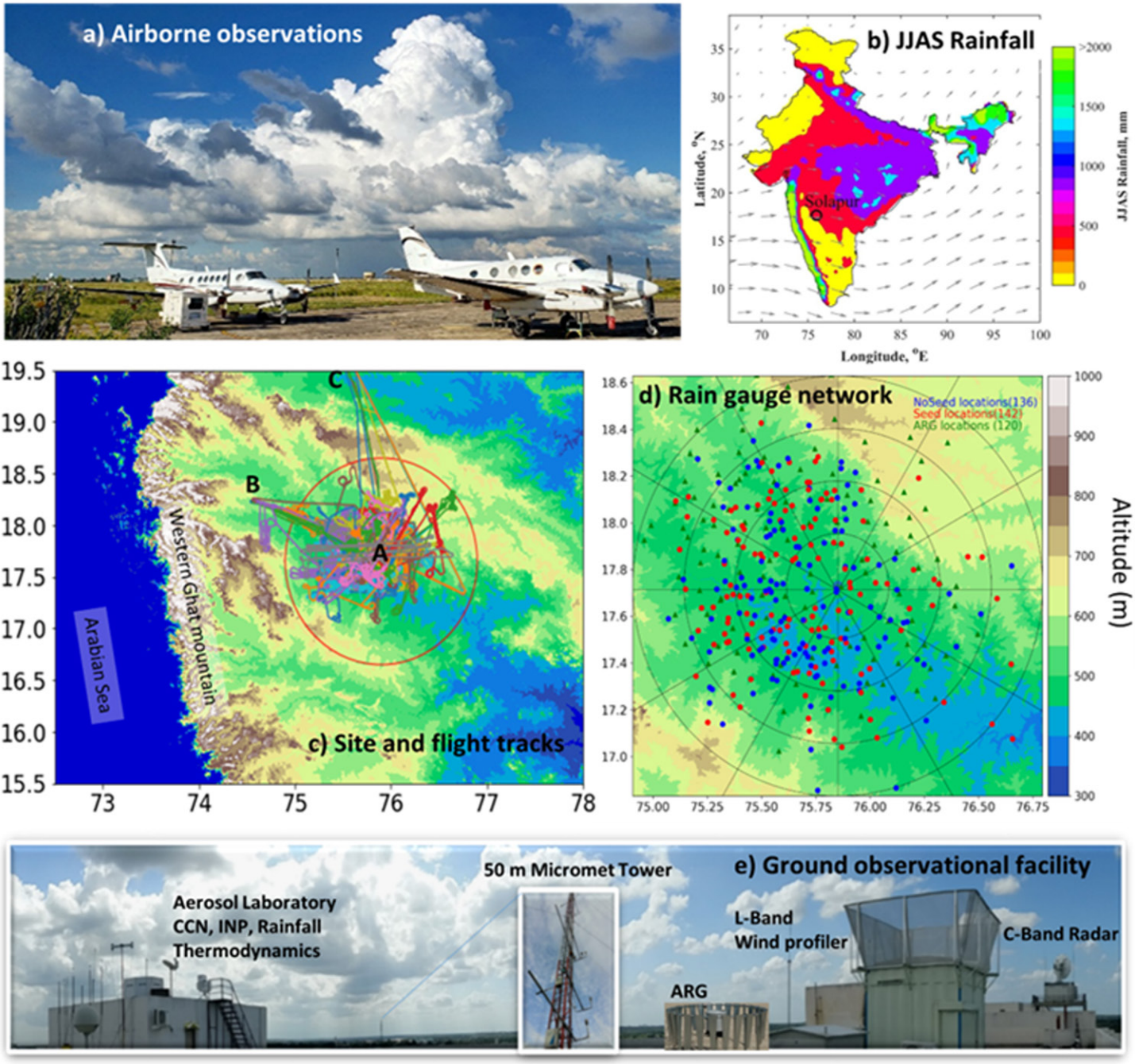

Fig. 1. (a) Photograph of the seeding and research-instrument aircraft. (b) Mean June–September (JJAS) rainfall climatology over India for the period 1900–2019 and at 0.25° × 0.25° resolution and 850 hPa wind based on the National Centers for Environmental Prediction (NCEP) reanalysis data (Pai et al. 2014). The experimental site, Solapur, is shown by the black circle. (c) Terrain elevation (color contours) with flight tracks. The letters labels—A, Solapur (17.62°N, 75.93°E); B, Baramati (18.22°N, 74.58°E); C, Aurangabad (19.86°N, 75.39°E)—indicate airports from where the aircraft was operated. (d) Automatic rain gauge (ARG) network and seeded locations and (e) the observational facilities at Solapur (17.73°N, 75.85°E).

Seeding hypothesis

- In hygroscopic seeding with supermicron flare particles (1–10 μm), cloud drop size spectra broaden near the cloud base, leading to enhanced drizzle formation aloft.
- The submicron-size flare particles delay the drizzle formation to above the freezing level, forming graupel, increasing riming rates, and accelerating precipitation.
- Seeding may also lead to extra area effects outside the seeded area in the monsoon environment under strong winds.

aerosol mass spectrometry to identify seed particle material in cloud hydrometeor residuals, and numerical simulations were conducted to test the seeding hypothesis.

The cloud seeding hypothesis, given in the sidebar "Seeding hypothesis," is that seeding particles at the cloud base delay rain formation in the clouds at lower levels, allowing drizzle to grow larger and produce precipitation more efficiently. The ambient CCN can initiate drizzle and rain at a lower level as cloud droplet spectra broaden and remove liquid water prematurely. Raindrops need to be large enough so they will not evaporate before reaching the ground. Hygroscopic seeding material, dispersed from burning flares, activates as large droplets and then grows by diffusion. Updrafts then loft the growing drops to the region of subzero temperatures (when the cloud top goes above the freezing level), where they can freeze heterogeneously and grow more rapidly through riming and aggregation, more efficient processes than warm rain formation. In addition, the ice splintering through the Hallet–Mossop process contributes to the growth of aggregates.

Convective clouds with a depth of a kilometer or more and likely to evolve into a cumulus congestus/deep cumulus were targeted in CAIPEEX. These clouds had cloud bases warmer than 0°C and cloud tops 2–3 km above the 0°C height (freezing level, henceforth) at an average altitude of 5 km. Suppose the seed particles are large enough compared to the background aerosols. In that case, the droplet size distributions (DSD) broadening may happen with an increase in cloud droplet effective radius with height and liquid water content (LWC), maximizing at greater altitudes and enhanced drizzle formation near cloud tops. When the seed particles are too small (in size) near the cloud base, droplet growth is suppressed due to the competition between many droplets. Hence, seeding strategically in time and space is critical to enhance rather than suppress precipitation.

Physical experiments to address the hypothesis of hygroscopic seeding were drawn from several previous CAIPEEX studies on aerosol–cloud interaction:

- With more CCN near the cloud base, there is a delay in the initiation of rain (Prabha et al. 2011; Konwar et al. 2012).
- The high liquid water content in less diluted cores leads to drizzle near cloud tops (Khain et al. 2013; Patade et al. 2019).
- Drizzle formed in warm cloud sectors can be transported to levels above freezing and participate in mixed-phase and ice-phase processes (Patade et al. 2019).
- More CCN in a highly moist environment can support greater precipitation (Gayatri et al. 2022).
- Additionally, extra area effects of the seeding may be anticipated (Gayatri et al. 2023).

Experiment design

The site and ground-based observations. The region targeted for cloud research and seeding has high water demand and is prone to frequent droughts. The climatological map of average rainfall over all of India for June to September (JJAS) (0.25° × 0.25° resolution) is shown in Fig. 1b for the period 1901–2019 (Pai et al. 2014). Solapur (17.73°N, 75.85°E,

population ~ 1 million), a city with low rainfall on the leeward side of WG (Fig. 1c), was chosen as the base of operations with automatic rain gauge (ARG) sites (Fig. 1d) within 100 km radius and an observational facility (Fig. 1e). The Solapur region receives less than 4.5 mm day^{-1} (460 mm of rainfall during JJAS). The region received 384 and 422 mm of accumulated rainfall from June to September 2018 and 2019, respectively.

A polarimetric, C-band radar (5.625 GHz; Selex/Leonardo Inc.) was sited to monitor precipitating systems and to aid the seeding operations. Other ground-based measurements at the observational facility included (i) physical, chemical, and hygroscopic properties of aerosols; (ii) vertical profiles of temperature, wind, and water vapor; (iii) rain measurements using rain gauges and disdrometers; (iv) ceilometers; and (v) a micrometeorological tower. More details on the various instruments are provided in Supplement B. Rainfall reaching the ground was measured with 120 telemetered, tipping-bucket-type rain gauges distributed over 100 × 100 km^2 around the ground site at Solapur. Rainfall was also measured with two disdrometers (one at Solapur and another at Tuljapur, 40 km in the northeast radar sector). Two microwave radiometer profilers (MWRP) provided thermodynamic information within the study area. The L-band wind profilers (1,280 MHz) registered horizontal and vertical winds from 200 m to 10 km. A 50-m-tall micrometeorological tower, installed at the northeast sector, within 2 km of the radar, monitored wind, temperature, and humidity at five levels using slow-response sensors. Eddy covariance systems were used to archive data at 10 Hz to document turbulent fluxes. In situ sensors also measured the physical, chemical, and hygroscopic properties of aerosols and CCN.

We also launched radiosondes (Vaisala model RS92-SGP) every day at 1100 Indian Standard Time (IST; 0530 UTC) to document the winds and thermodynamic conditions of the background atmosphere. The monsoon onset was marked by the strengthening of the tropical easterly jet (TEJ) in the upper troposphere (Fig. 2b) and the low-level jet (LLJ) (Fig. 2c), which brought an influx of moisture to the continental Indian region. The episodic variations of westerly LLJ (bringing moisture from the Arabian Sea), in its strength and vertical extent (Fig. 2c), generally coincided with more rainfall (Fig. 2a) over the Indian region. A northwesterly wind component is noted over Solapur region at 2 km altitude (Fig. 2c). The monsoon rainfall over the region shows a northward propagation feature (Fig. 2a), a typical characteristic during the monsoon season.

The strengthening and appearance of easterlies in the lower layers indicated dry conditions. The precipitable water and the liquid water path (Fig. 2d) are typically enhanced during a dry–wet transition period in June and September and within the monsoon break periods. The convective available potential energy (CAPE), observed at noon (not shown), was seen to exceed 1,000 J kg^{-1} on most days and diminish during nonmonsoon periods. The freezing level was around 4.5–5 km (Fig. 2e). The lifting condensation level (LCL), planetary boundary layer height (PBL), and cloud base (CB, more variable during break) were located around 1.5 km (Fig. 2e) AGL, and the monsoon LLJ peaked above this level. There were predominantly congestus (with a warm cloud base and cold tops up to 4–9 km) and cumulonimbus clouds (with tops exceeding 9 km) during the monsoon, while cumulus-type clouds (with cloud tops up to 4 km) increased toward the end of the monsoon season (Fig. 2f). The dip in the ambient CCN concentration during the monsoon months is seen in the observational data of 2 years at the site (Fig. 2g). The CCN concentrations are maximum during June and September when dry conditions are present. A summary of findings from all aerosol measurements at the ground site is provided in Supplement B1.

Airborne observations. A research aircraft (RA; Beechcraft King Air B200) and a seeder aircraft (SA; Beechcraft King Air C90) were used for airborne in situ measurements and seed material dispersal, respectively (Fig. 1a). Wing- and cabin-mounted instruments were used

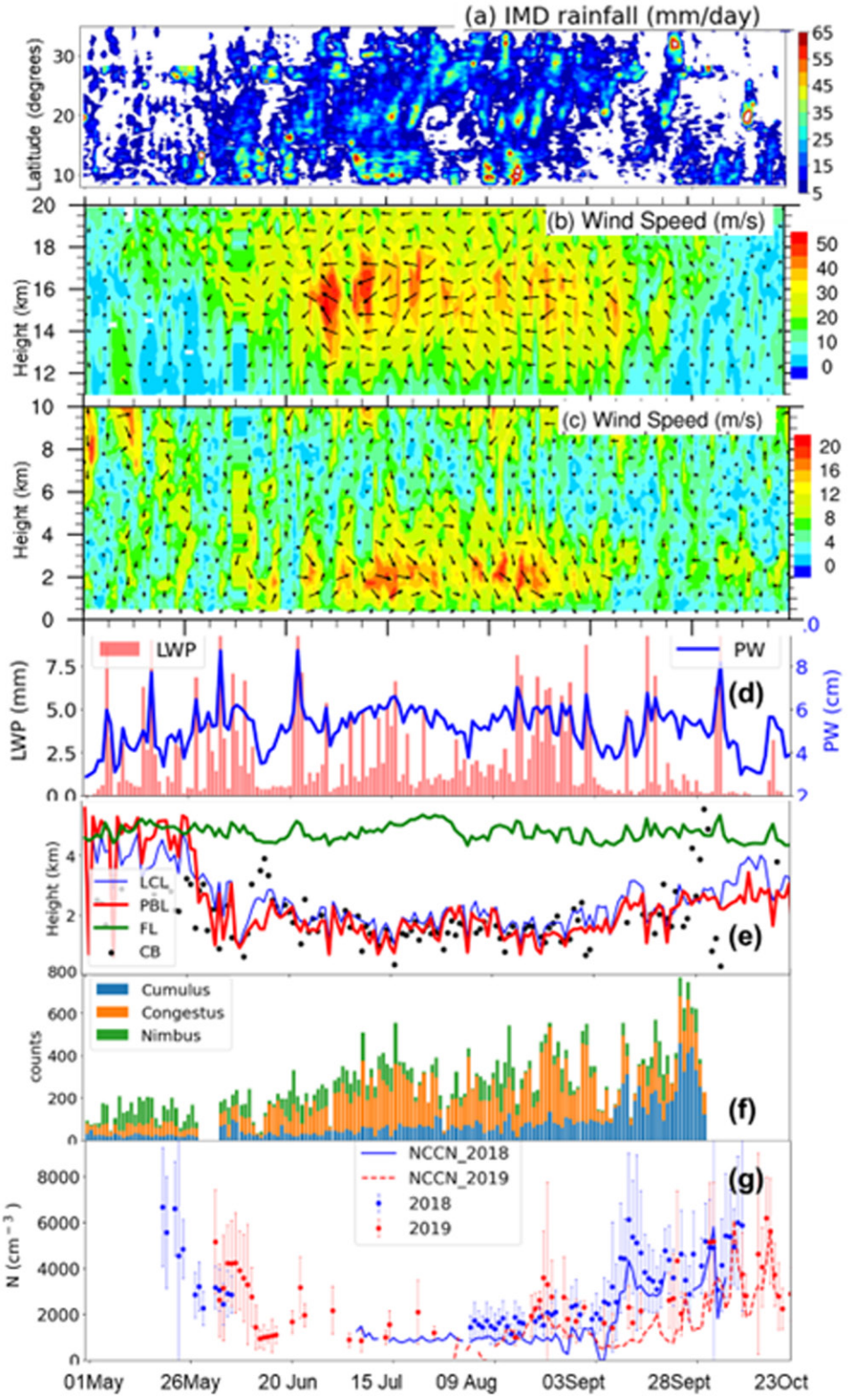

Fig. 2. Time series of various parameters observed at the ground site from 1 May to 23 Oct 2018. (a) The rainfall (mm day^{-1}) Hovmöller plot, (b) winds indicate the upper-level jet, and (c) the low-level jet from radiosonde measurements during the monsoon season in 2018 at 1100 IST (0530 UTC). (d) Daily maximum value of liquid water path (LWP; mm) and precipitable water (PW; cm) from the MWRP and (e) variation of lifting condensation level (LCL; km), planetary boundary layer height (PBL; km), freezing level (FL; km), and cloud-base height (CB; km) from MWRP. (f) Different cloud types identified using the C-band radar observations and (g) daily-average surface aerosol concentrations (symbols) from SMPS and CCN concentration (at 1% SS; cm^{-3}) and number concentration of CCN (NCCN; indicated with line) measured during the campaign period using DMT CCN counter. Error bars indicate the variability during the day, where present.

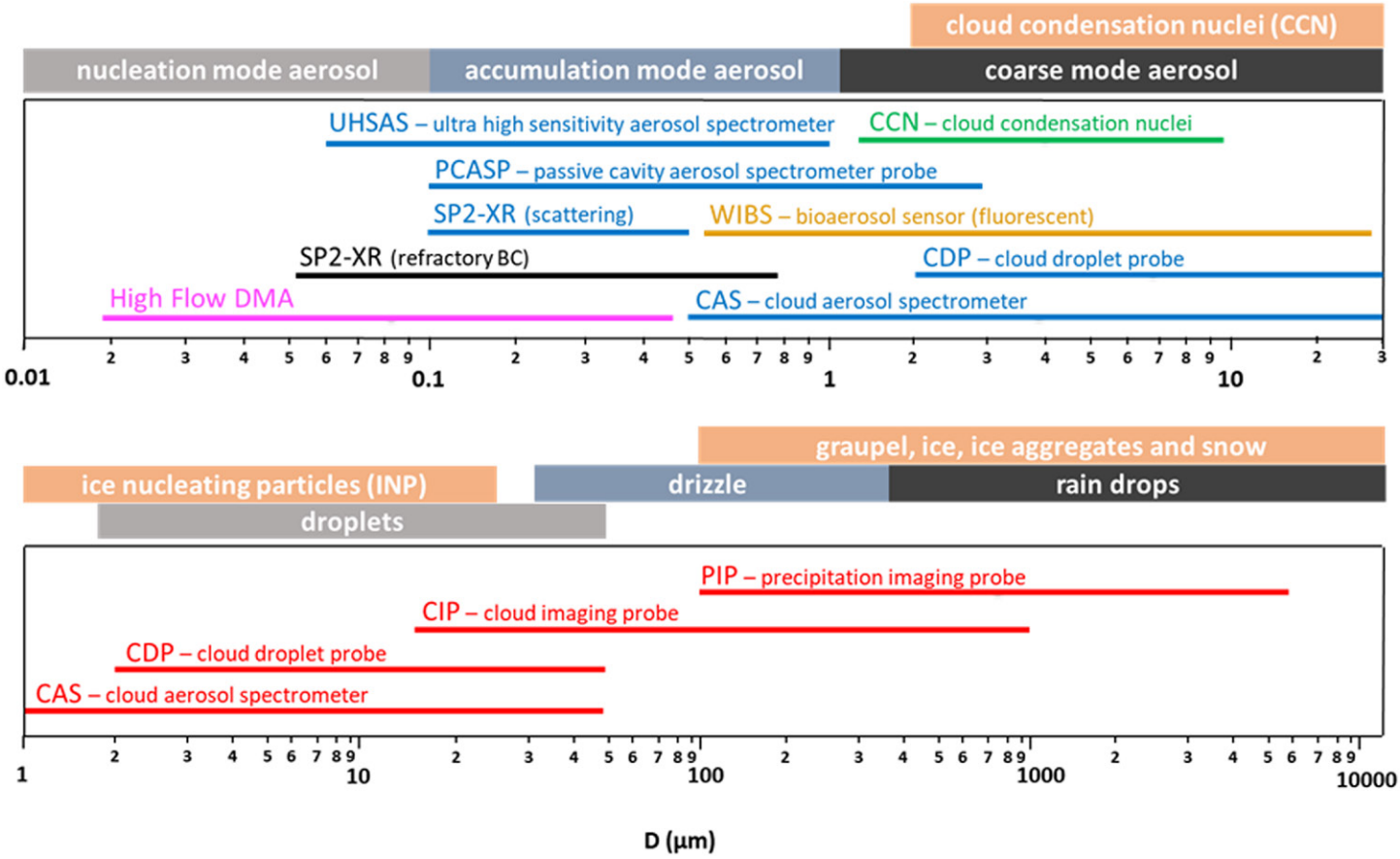

Fig. 3. Ranges of various airborne particle-sizing instruments used in CAIPEEX IV.

on both aircraft. Figure 3 illustrates the instruments on the aircraft with their size ranges. Measurements of microphysical properties were collected in convective clouds, and the range of instruments (Supplement C gives various acronyms of instruments, accuracy, size ranges, etc.) used in the experiment allowed documentation of the size distributions of aerosol particles and cloud hydrometeors from a few nanometers to several millimeters. Specific data quality control procedures were used to ensure artifact-free measurements and minimize instrument limitations, as described in Supplement C, which also provides the layout of the instruments on the RA (Fig. C1). The particulate chemistry measurements on a few flights identified the seeding signature with a mini aerosol mass spectrometer (AMS) (Goetz et al. 2018; Werden et al. 2022).

The scanning differential mobility analyzer (DMA), sampling in the aircraft cabin from an aerosol inlet, provides the best measure of particles in the 0.02–0.5 μm diameter range. The DMA measurements are complemented with those from the passive cavity aerosol spectrometer probe (PCASP), which detects particles from 0.12 to 3 μm, from the ultra-high-sensitivity aerosol spectrometer (UHSAS) that covers the 0.05 to 1.0 μm range and the Cloud and Aerosol Spectrometer with Polarization (CAS-POL) that measures from 0.5 to 50 μm. These overlapping size ranges capture the expected size range of both ambient and seeding CCN. Observations were carried out with the RA and SA depending on each mission's objective. Clouds were sampled at different altitudes before and after seeding. A typical cloud profiling research strategy is given in Supplement C.

C-band radar observations (Samanta et al. 2021) helped in selecting suitable clouds to seed, guided both aircraft using telemetry, and monitored precipitation development after seeding. Precipitation was also measured with the rain gauge network. During the 2018 experiment, flights took off from three nearby airports (Solapur, Baramati, and

Aurangabad, indicated in Fig. 1c as A, B, and C). In contrast, all the flights were conducted from the Solapur airport in 2019.

The vertical profiles of refractory black carbon mass [rBC using the Single Particle Soot Photometer Extended Range (SP2-XR)] and fluorescing biological aerosol particle (FBAP) concentrations, using the Wideband Integrated Bioaerosol Sensor (WIBS), were measured for the first time during the Indian monsoon. These datasets will help to understand the cloud direct and indirect effects of these particles in the monsoon environment.

As per the Glossary of Meteorology, the size range for drizzle is defined here as 200–500 μm; the size range for precipitation is >500 μm (American Meteorological Society 2023). The Cloud Imaging Probe (CIP) measured the drizzle-sized droplets, and the Precipitation Imaging Probe (PIP) measured raindrops and larger ice crystals. All aircraft data analyses correspond to the maximum values and 90th percentile of cloud parameters observed with each cloud penetration (defined as ≥10 s within the cloud) at varying altitudes.

Forty-eight RA flights were conducted in 2018 and 58 in 2019. Forty-one SA flights were conducted in 2018 and 62 in 2019 for 480 h of aircraft observations during the 2 years. Eighty-three randomized seeding samples were collected in 2018 and 195 in 2019, totaling 278 hygroscopic seeding samples in CAIPEEX IV. Two hygroscopic cases are not considered in this study due to a lack of radar observations.

Aerosol vertical profiles. Four categories of aerosol particles measured during the experiment are presented in Fig. 4. All light scattering particles (from the PCASP and UHSAS) in the equivalent optical diameter (EOD) range 0.06–3.0 μm, CCN activated at 0.5% supersaturation (SS), rBC (from the SP2-XR), and FBAP (from the WIBS). The close correspondence between the CCN and UHSAS concentrations (Fig. 4a) indicates that the CCN activated at 0.5% SS are particles larger than the lower threshold of the UHSAS (0.06 μm). A study of CCN closure and aerosol size distributions during CAIPEEX is reported by Varghese et al. (2023). The FBAP, which was measured for the first time over the Indian region, shows a similar trend with altitude as with the other measurements. The high values of rBC aerosols around the 4–5 km layer in 2018 corroborate with CALIPSO measurements (Supplement Fig. B2). There is also nonlocal transport with a contrasting aerosol feature above the boundary layer with a marine aerosol signature (Varghese et al. 2021). The vertical profile of ambient aerosol chemical composition from the mini-AMS measurements (Fig. 4b) shows a predominant organics contribution, followed by nitrates (which are nearly constant with altitude) and sulfates.

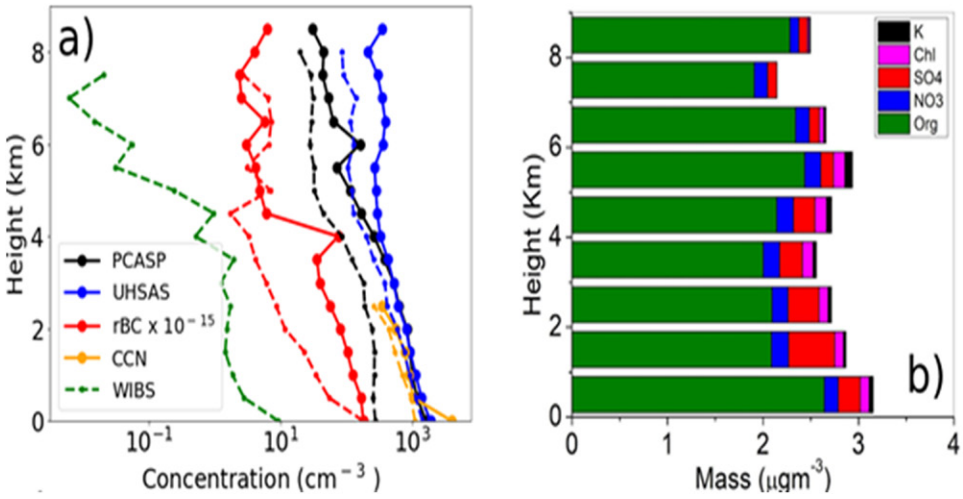

Fig. 4. (a) Aerosol number concentration, CCN, and different aerosol observations in 2018 (continuous lines) and 2019 (dashed lines). (b) Aerosol chemical composition as observed during the experiment, averaged for all flights.

Cloud properties. The southwesterly winds were found to be stronger and deeper in 2019, compared to 2018, related to the stronger Indian monsoon in 2019 vis-à-vis 2018 (Supplement Fig. C2), which has a significant impact on the cloud properties as illustrated in Fig. 5. The vertical profiles of cloud microphysical properties in Fig. 5 show the average of the maximum values of all sampled clouds, along with the standard deviation about the means and the 90th percentiles. Note that most of the cloud penetrations were conducted in the developing convective clouds (which means without precipitation at the cloud base). The average cloud width (Fig. 5a), as an estimate of the length of cloud penetrations and the time in the cloud [with cloud droplet number concentration (CDNC) > 20 cm^{-3}], is large in 2019. The year 2019 has deeper clouds with stronger vertical growth and greater widths, probably due to more moist conditions. The maximum updrafts (Fig. C2) are stronger than 2 m s^{-1} in several cloud passes in both years.

As expected, in liquid-dominated convective clouds, the maximum liquid water content (LWC; g m^{-3}; Fig. 5b) increases with altitude, and the CDNC (cm^{-3}; Fig. 5c) reaches a maximum at 2–3 km and after that decreases due to collision coalescence, accretion, and fall out. Maximum CDNCs in 2018 are almost a factor of 2 larger than 2019, and maximum cloud droplet probe (CDP) mean volume diameters (MVDs) are approximately a factor of 2 smaller (within ±20%). In addition, the maximum MVDs from the PIP in 2018 were 50% smaller than in 2019. No significant differences exist in the average cloud-base CCN concentrations between the 2018 and 2019 observations (Fig. 4a) or in the maximum LWC.

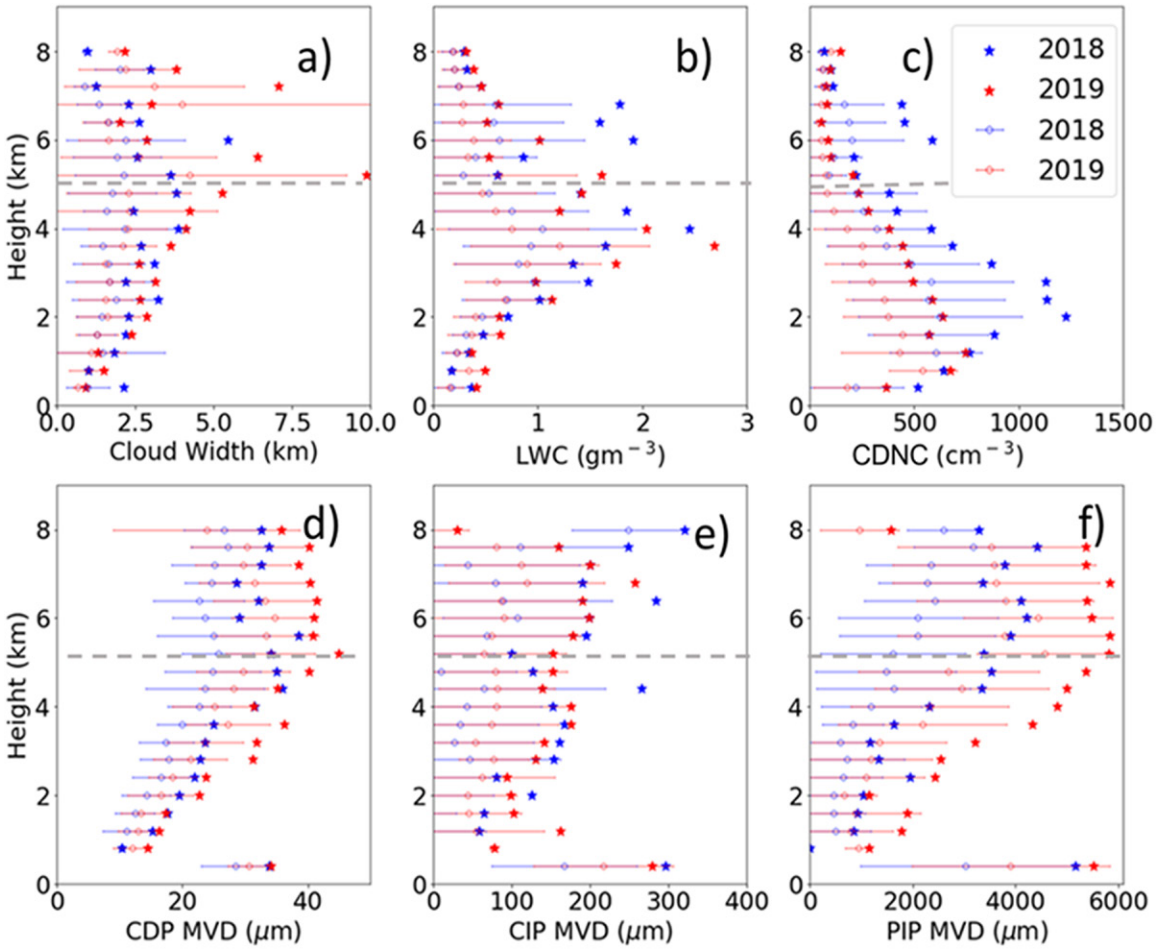

Fig. 5. Vertical profiles of the average maximum values for (over several cloud passes) sampled clouds in 2018 (blue) and 2019 (red) of different cloud properties. The horizontal bars are ±1 standard deviation, and the stars indicate the 90th percentile. (a) Cloud width; (b) liquid water content; (c) droplet number concentration; (d) CDP mean volume diameter; (e) CIP mean volume diameter; (f) PIP mean volume diameter. All data are maximum values from each cloud penetration and then averaged for all flights at respective altitudes where observations were taken. The dashed line is the freezing level.

The drizzle and precipitation MVDs, derived from the CIP and PIP measurements, respectively (Figs. 5e,f), and PIP show a steep increase from around the average cloud base of 1,000 m to their maximum values at or above the average freezing level at 5 km. This peak is attributed to the precipitation formation due to the development of ice hydrometeors. The vertical profiles of LWC, CDNC, and CDP MVD (Figs. 5b–d) are the expected microphysical signatures. The MVDs from the CDP, CIP, and PIP continue to increase. This results from collision and coalescence below the freezing level, then depositional, riming, and aggregational growth of ice crystals above. Large aggregates/drops are found in the mixed-phase region, peaking around 6 km, and PIP MVDs in 2019 were significantly larger than in 2018 (Fig. 5f). Further case-by-case investigation with a detailed investigation of cloud microphysical parameters is warranted.

Strategy for hygroscopic seeding in warm base clouds. Based on the evaluation of previous measurements in this region of the ambient CCN population and the vertical profiles of temperature, humidity, and winds, we set the criteria for seeding as 1) a well-defined cloud base with no precipitation falling at the time of seeding, 2) a maximum value of LWC ≥ 0.5 g m^{-3} at 300 m above the cloud base, and 3) maximum updrafts > 1.5 m s^{-1} at the cloud base. Another notable signature we investigated is the warm-layer depth (freezing level – cloud-base height), which is linearly related to the cloud droplet effective radius (see more details on the availability of warm-layer depth over the region, described in Supplement B5) over the rain-shadow region (Patade et al. 2019). This allows large drops to enter subzero temperatures and contribute to ice particle formation (note that we have predominant congestus clouds with cloud tops reaching 9 km, as shown in Fig. 2f). Hence, we set the criterion that the warm-layer depth of clouds should be >1 km for considering the seeding operations in convective clouds.

Summary of the experiment

Cloud seeding flare characterization. Both aircraft were equipped with cloud seeding flares (Ice Crystal Engineering LLC). The RA had the provision for mounting hygroscopic, burn-in-place (BIP), and ejectable glaciogenic flares (EJ). The hygroscopic flare composition used in the present experiment combines calcium chloride and magnesium, with potassium perchlorate as a binder. A flare burns for approximately 4 min. Hygroscopic cloud seeding flares, when burned near the cloud base, release a large concentration of hygroscopic $CaCl_2$ aerosols in the size range of 90–500 nm. During the flare-testing experiment (details are given in Supplement C3), the background CCN measured was around 600–800 cm^{-3} and 2,000–3,000 cm^{-3} at 0.1% and 0.56% supersaturation, respectively (Fig. 6). The CCN concentrations from the flares were 10,000 cm^{-3} at 0.1% and 40,000 cm^{-3} at 0.56% supersaturation within 200 m of the flare source. Additionally, the number concentrations measured in the 2-flare (2F) and 4-flare (4F)

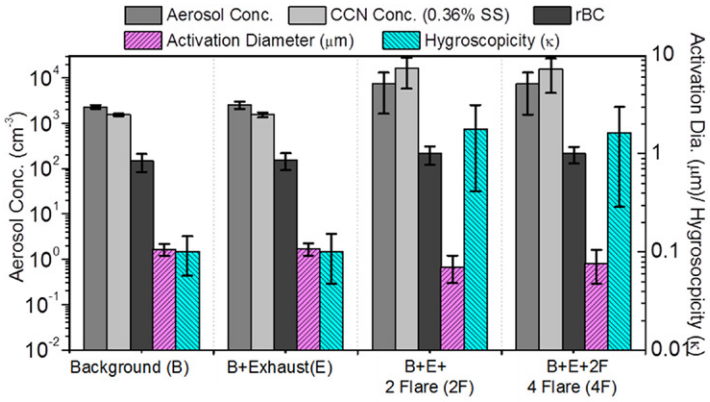

Fig. 6. The number concentrations of total aerosol (60 nm–3 μm), CCN at 0.36% supersaturation, rBC aerosols, apparent activation diameters (μm), and single hygroscopicity parameter (κ) estimated during the sampling of background (B), aircraft exhaust (E), and 2-Flares (2F) and 4-Flares (4F) burning. The error bars denote the standard deviation due to spatial variations.

burning experiments were nearly the same (this could be due to the detection limit of the instrument). This needs further investigation to comment on this result. The CCN number concentrations at 0.36% SS were higher than the aerosol (60 nm–3.0 μm) concentrations during the flare samplings, indicating the high hygroscopicity of the fine aerosols emitted from the flare.

Compared to the background, the flare introduced many additional aerosols in the 50–200 nm size range with a peak at 100 nm. The single hygroscopicity parameter (κ) was estimated from the aerosol and CCN number concentrations (Petters and Kreidenweis 2007). The mean apparent activation diameter is around 100 nm during background and exhaust sampling, while it reduces to 60–70 nm during the flare sampling. The mean bulk hygroscopicities increased from 0.1 during background and exhaust sampling to above 1 during the flare sampling.

Tracking the seeding signature of flare seeding particles. One fundamental issue with flare seeding is that their particles are needed in large quantities to identify their signature within the chain of cloud microphysical processes from seeding to precipitation (Rosenfeld et al. 2010). Their study indicated that "the actual measurements failed to identify a clear microphysical seeding signature from the burning of hygroscopic flares within the seeded convective clouds," compared to stratiform clouds (Ghate et al. 2007). Hence, it is important to have a reliable method to track the seeding material and investigate the cloud microphysical properties associated with the seeding signature. This is mainly a challenge in convective clouds due to the significant variability in the cloud dynamics that include strong vertical motions, entrainment, and mixing. Two new methodologies were evaluated for identifying seeding signatures within clouds. Both methodologies compare selected chemical properties of aerosols in cloud-free air with those of cloud hydrometeor residuals. The rBC number and mass concentrations were measured with SP2-XR. The masses of selected inorganic and organic ions were measured with a compact aerosol mass spectrometer (mini-AMS). Both were sampled from the airstream behind a Counterflow Virtual Impactor (CVI) inlet with a cut size of 7 μm diameter (removes gases and aerosols below this size). When the aircraft was in cloud-free air, the instruments sampled from a total aerosol inlet, and when in the cloud, the instruments were switched to the CVI.

The SP2-XR measures not only the incandescence from particles containing rBC, but also scattered light from individual particles, 100–500 nm in EOD. Figure 7a summarizes the average values of the CCN number concentrations at 0.5% SS, single-particle light scattering number concentrations from the PCASP, UHSAS, and SP2-XR, and number concentrations of rBC as described for the aircraft observations of several clouds and their environment from Gayatri et al. (2023). In comparison, concerning the SP2XR measurements, Figs. 7b and 7e compare the number concentrations of all light scattering and incandescent (rBC) residuals from the SP2XR behind the CVI for seed and no-seed cases, respectively. Given that many studies have shown that fresh rBC is poor CCN until the rBC is aged, the relatively large concentrations of rBC, >100 cm^{-3} in the cloud residual, imply that these are aged rBC particles. In addition, there is no significant difference in the seed and no-seed concentrations of rBC, nor should we expect there to be differences since the flares do not produce black carbon. In contrast, the average number concentrations of all light scattering particles in the residuals more than double, and the standard deviations quadruple from no-seed to seed conditions.

A mini-AMS was used to identify the chemical signature of seeding aerosols and sampled cloud residual particles behind a CVI. Figure 7c indicates observations taken near the cloud base on several flights while outside the cloud (with CDNC < 20 cm^{-3}) and inside the cloud (with CDNC > 20 cm^{-3}) before and after seeding at the cloud base (seeding was done at the

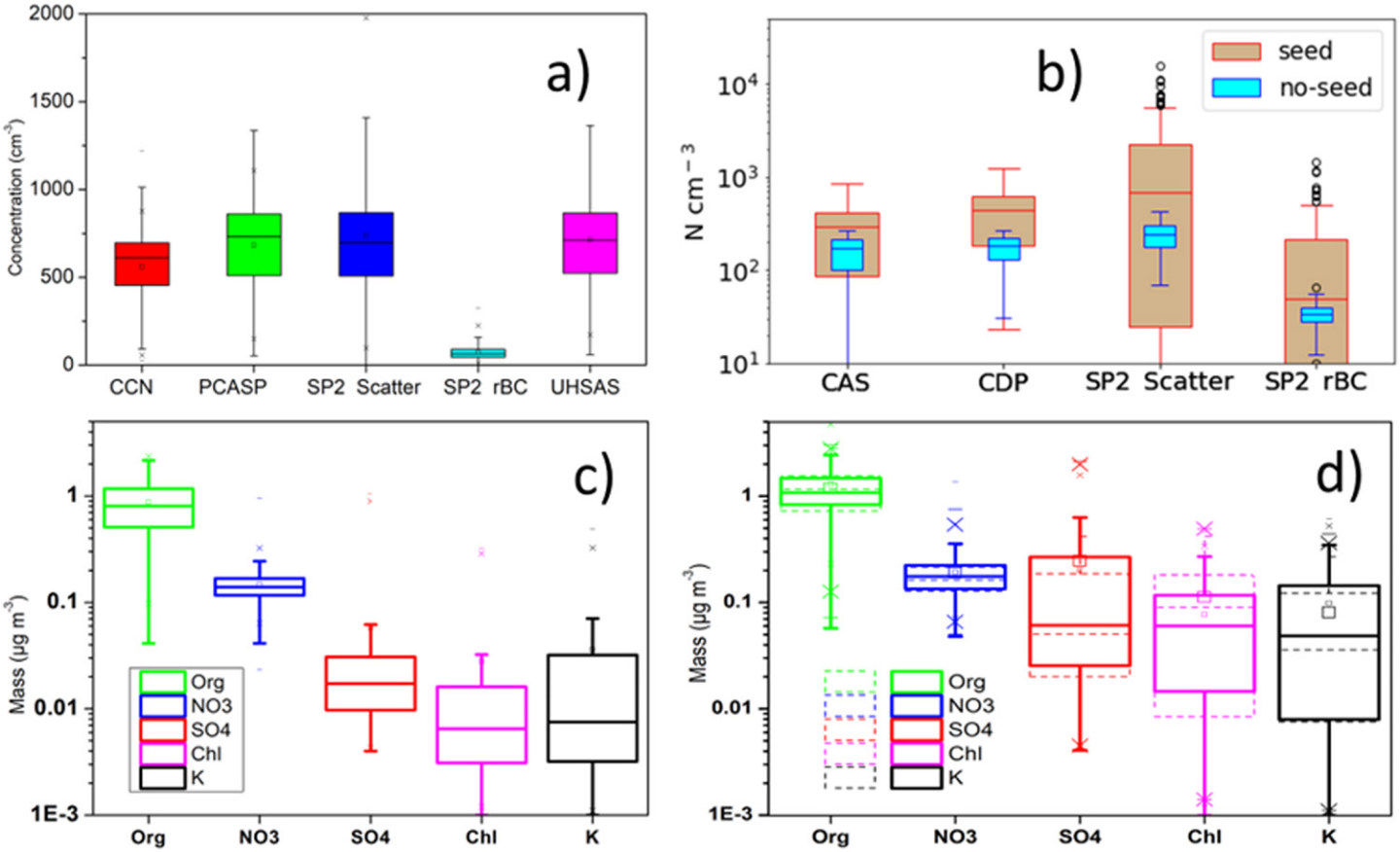

Fig. 7. (a) Ambient number concentration of CCN, aerosol 0.12–3 μm EOD (PCASP), SP2-XR light scattering particles (0.1–0.5 μm EOD), SP2-XR refractory black carbon mass concentration (rBC), and aerosol 0.06–1 μm EOD (UHSAS) near the cloud base before seeding; rBC is in femtograms (fmtg), thus multiplied by 10^{-15}. (b) Concentrations of cloud hydrometeors measured with the CAS and CDP and SP2-XR light scattering and rBC in residuals before and after seeding. These results are after two seeding events near the cloud base. Mini-AMS observations of organics, nitrates, sulfates, chloride, and potassium (c) outside and (d) inside cloud residuals. Dashed lines indicate the cloud pass before sedding, and thick lines show the cloud pass after seeding. In the box-and-whisker plots, the horizontal lines within the box represent the mean, and the upper and lower lines represent the 75th- and 25th-percentile values, respectively, whereas the lower and upper horizontal lines outside the box show the minimum and maximum values, respectively. The symbols give outliers. The error bars denote the standard deviation due to spatial variations.

cloud base at 1.8 km). The mass concentration of chlorine (Cl) and potassium (K) (μg m^{-3}) along the aircraft transects was documented for the seed and no-seed clouds. The mass concentration of aerosol SO_4 and K increased while Cl decreased in the seeded cloud droplet residuals compared to no-seed cloud residuals (Fig. 7d). Aqueous chemistry modeling of aerosol and droplet growth from CAIPEEX indicates that mildly soluble, wet-haze droplets can facilitate the formation of sulfate over droplets (Gumber et al. 2022). This is one possible reason for observing the increasing mass concentration of sulfate in seeded cloud residuals. Meanwhile, potassium is used in the flare as a burning reagent, which is the likely source of its increase. The chemical signature of seed material was found up to an altitude of 4 km, which is 2.2 km above the cloud base. Seeding was done at 1.8 km, suggesting that 1) strong updrafts transport seeded particles more effectively within clouds to higher altitudes and 2) there was a change in the cloud microphysical properties.

Seeding impact evaluation. The seeding impact evaluation aims to identify changes in cloud properties detectable from in situ measurements. The same conditions indicated in the sidebar "Seeding criteria" are used in the physical and randomization experiments. Initially, the aircraft made a cloud penetration at 300 m above the cloud base to investigate LWC and looked for updrafts near the cloud base > 1.5 ms^{-1}. When complementary

Seeding criteria

The selection of convective clouds for seeding is based on the following conditions:

1) A well-defined cloud base with no precipitation at the time of seeding.
2) A LWC > 0.5 g m^{-3} at 300 m above the cloud base.
3) The updraft > 1.5 m s^{-1} at the cloud base.
4) The warm-layer depth (freezing level − cloud-base height) > 1 km.
5) 2–6-km-layer tropospheric RH > 40%.

Note: Operational strategy depended on hourly, 1 km numerical model forecasts (Gayatri et al. 2022), radiosonde ascent 1 h before the flight, and ground-based C-band radar observations (Samanta et al. 2021) during the flight to select the seeding sector.

conditions for seeding were identified as in "Seeding criteria," the cloud was then selected, and seeding took place with two flares burning on each wing for nearly 4 min while the aircraft took a circular flight track below the cloud base. Whether seeding was done or not on the candidate cloud depended on the random decision as per the randomization procedure.

The identifiers in the seeding hypothesis include 1) seeding signature as indicated in the previous section, 2) the presence of high CDNC in response to seeding, 3) changes in the DSD at 300 m above cloud base, and 4) drizzle formation within clouds after seeding as in Tessendorf et al. (2012). The cloud seeding flares are burned in cloud-base updrafts so the seed particles can enter clouds with minimum dispersion. The experiment has documented several cloud penetrations with updrafts > 2 m s^{-1} and LWC > 0.5 g m^{-3}. In the physical experiment, the aircraft made several cloud penetrations at different altitudes (as indicated in Supplement Fig. C1). It may also be noted that while at the cloud base, the aircraft avoided sampling the seeded plume (except for the dedicated missions for flare sampling). This was done to prevent excessive particle load on the sensors.

We have investigated the aerosol number concentrations from the UHSAS and CCN near the cloud base at 0.4% SS and the CDNC within 300 m above the cloud base in updrafts > 2 m s^{-1}, both before and after seeding (Figs. 8a,b). The comparison of the UHSAS concentrations with the CDNC indicates that many submicron particles are participating in the cloud formation. Additionally, in a few instances, a very polluted (with high CCN) cloud base (while aircraft sampled seeded plume) and many droplets are noted concurrently.

The cloud droplet MVD (Fig. 8c) is used as a metric for characterizing the median size of droplets related to the LWC at different altitudes. These observations showed 10 μm MVD droplets close to the cloud base in most observations, corresponding to a number concentration of droplets > 500 cm^{-3}. A large number concentration of cloud droplets corresponded to a high aerosol number concentration at the cloud base. The droplet growth is slowed in the higher aerosol concentration environment (seeded cases), clouds have greater depth, and precipitation comes from altitudes where the temperature is below zero. The clean clouds (with droplet number concentration < 500 cm^{-3}) develop raindrops and drizzle drops at a lower altitude (see Fig. 8c). Figure 8d illustrates samples from several seed and no-seed clouds of small (2–20 μm) and large cloud droplets (20–50 μm). Small and large droplets after seeding are significantly larger than the no-seed samples. This finding suggests that seeding has increased both the small and large droplet populations, which is ideal for collision–coalescence. This behavior is observed for a range of cloud-base heights. In stratiform clouds (Ghate et al. 2007), the impact on cloud microphysics due to large-size seed particles was documented, and the unexplained variability pointed to the vertical velocity and its inhomogeneity.

The high CDNC clouds have an advantage over the lower CDNC clouds due to the delay in precipitation development as per the seeding hypothesis, and large drops are seen in

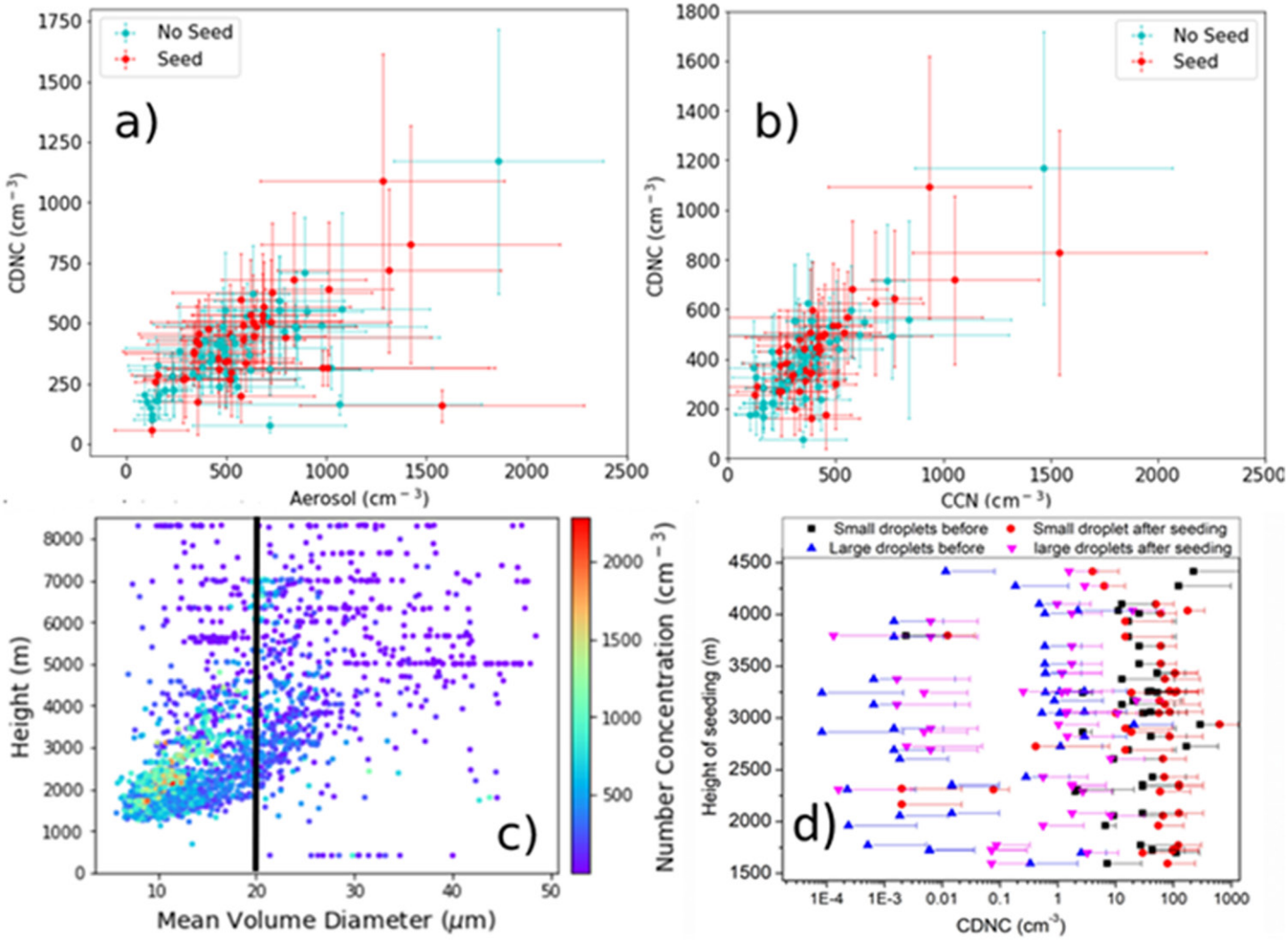

Fig. 8. (a) Scatterplot of UHSAS aerosol concentration vs CDNC and (b) CCN at 0.4% SS at the cloud base vs the CDNC at 300 m above the cloud base from several cloud penetrations before and after seeding. (c) Vertical variation of cloud droplet MVD from several cloud passes and corresponding droplet number concentration (color). (d) Variation of small (D < 20 μm) and large (D > 20 μm) cloud droplet number concentration with height in the cloud volume before and after seeding, indicating the broadening of the DSD in the small and large sizes from several seed and no-seed cloud samples. The vertical line in (c) is D = 20 μm. The error bars denote the standard deviation due to spatial variations, which include diluted and undiluted cloud parcels over a distance of 50 km.

the mixed-phase region. The cloud-base seeding enhanced small and large droplet number concentrations within the cloud, suppressing collision–coalescence at lower levels and also leading to more collisions subsequently. This enhances the supercooled liquid and delays precipitation development.

Randomized experiment. Based on the seeding criteria (sidebar "Seeding criteria"), we conducted the randomization experiments (Supplement D1) by selecting similar clouds in seeded and unseeded categories in different environments. The 276 selected, randomized cases, which resulted from various environmental conditions prevailing over the site and their overall outcome, are presented in the sidebar "Outcome of CAIPEEX IV randomized experiments using radar." A double-blind procedure, discussed in Supplement D1, was followed while collecting these data. A detailed analysis procedure was followed for the rainfall observations [from Automatic Rain Gauge (ARG) and radar] downwind of the seeded area within 2 h after seeding, as described in Supplement B.

Outcome of CAIPEEX IV randomized experiments using radar

Table SB1. The outcome of CAIPEEX IV randomized experiments using radar. Note that the maximum reflectivity of 30 dB*Z* from the radar was not a criterion for seeding due to the time delay of 6 min between the radar scans. This table is made by investigating each case with radar data. Note also that one seed sample and three no-seed sample radar data were not available for evaluation.

Category	Total of 276 randomized samples in convective clouds for hygroscopic seeding	Seeded number (%)	Not-seeded number (%)
A	Total number of cases	150 (54.7%)	122 (45.3%)
B	Clouds dissipated, and no rain	83 (55.0%)	86 (68.8%)
C	Cloud developed, no rain	8 (5.3%)	5 (4.0%)
D[a]	<30 dB*Z* at the time of seeding and developed rain after seeding	31 (20.5%)	14 (11.2%)
E[a]	>30 dB*Z* at the time of seeding and developed rain after seeding	29 (19.2%)	20 (16.0%)

[a] A detailed evaluation of these cases is provided in Supplement D3.

We conducted five different analyses of the randomized cases: 1) evaluation of the vertical structure of seed versus no-seed samples using radar observations, 2) checking of the sample mean with bootstrapping analysis of rainfall from ARG and radar observations, 3) Monte Carlo (MC) simulations of the seed and no-seed samples from ARG data, 4) evaluating the relative enhancement in the 100 km^2 downwind area of seeding, and 5) quartile analysis of time histories of seed and no-seed samples from radar observations.

Evaluation of the cloud vertical structure from radar observations. Vertical profiles of reflectivity (dB*Z*) measurements from C-band weather radar are presented (Fig. 9) in the form of frequency-by-altitude display (FAD) (Yuter and Houze 1995) and following the analysis procedure introduced by Geerts et al. (2010). The methodology, described in Supplement B3, uses 276 randomized samples, 151 seeded and 125 not seeded (1 seed and 3 no-seed samples were without radar observation, thus making 150 seed and 122 no-seed samples from radar for evaluation). The maximum percentage of reflectivity pixels (more than 45%) lie below the 10 dB*Z* range and 4 km height in both seed (Fig. 9a) and no-seed (Fig. 9b) cases. The lower region (below 4 km) has about 63% of cloud pixels in seed samples and 68% in the no-seed samples. Comparing higher-altitude values (above the freezing level of 5 km), the seed cases have more pixels than no-seed cases.

Figure 9c is the difference between the seed and no-seed number frequencies (i.e., Fig. 9b pixel frequency subtracted from Fig. 9a pixel frequency). Negative (positive) numbers in the boxes in Fig. 9c indicate a reduction (increase) in cloud pixels within the marked region. Whereas the lower altitudes below 4 km largely show a reduction in the number of pixels, the higher altitudes show an increase in number of cloud pixels. Also shown in Fig. 9c is the average reflectivity profile in seed and no-seed cases. Although the difference in the number of pixels shows positive or negative, the mean reflectivities remained slightly higher in seeded cases. Figure 9d is the relative change in rain rate derived from the radar, calculated as (seed – no seed)/no seed. The rain rate (R; mm h^{-1}) is calculated using the standard Marshall–Palmer relation $Z = 200R^{1.6}$, and it is shown in the upper abscissa of Fig. 9d. This may be different for the different rain types, and a unified relationship may be established.

The hygroscopic seeding with a large CCN may initiate raindrops very close to the cloud base, while the small CCN may delay precipitation as per our seeding hypothesis. This also leads to the appearance of higher LWC at higher altitudes, and crossing the freezing level introduces more ice particles. The seeded sample analysis showed enhancement of more pixels in higher reflectivity (>25 dB*Z*) at higher altitudes. The rain rate relative enhancement

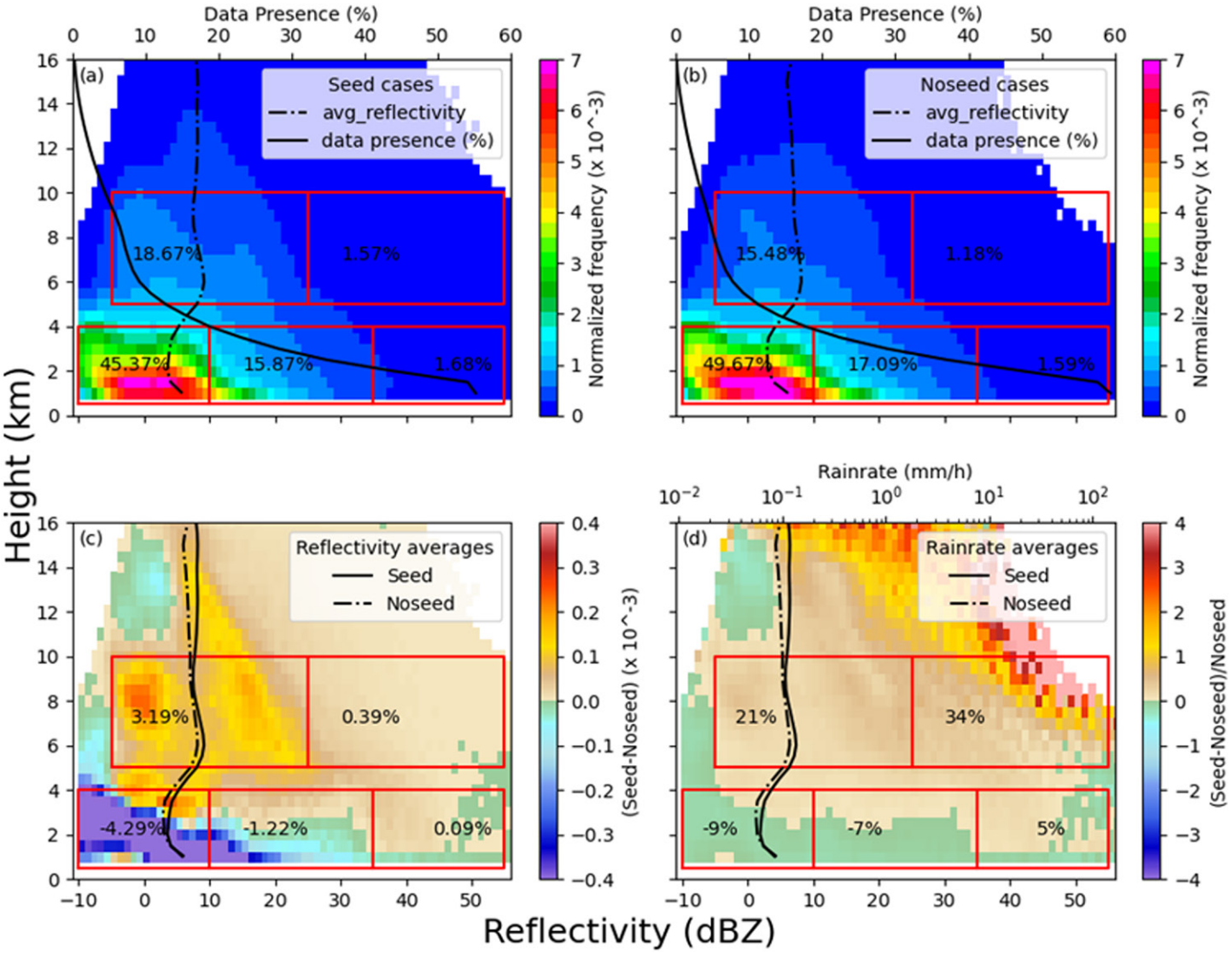

Fig. 9. FAD diagram of reflectivity values of seed and no-seed cases. (a) Occurrences of cloud pixels at 1 dB*Z* bin interval against height AGL for seed cases. The data presence (%) at each height is shown in the upper abscissa. The mean reflectivity profile is also shown. This analysis includes all the profiles in the downwind direction from seed time to the 1-h interval. (b) As in (a), but for no-seed cases. (c) The difference between data in (a) and (b), i.e., seed – no seed; the average profiles from (a) and (b) are also shown. (d) The relative change in rain rate (seed – no seed)/no seed.

in the region between 5 and 10 km is 21% and 34%, respectively, for the reflectivity <25 and >25 dB*Z*. The enhancement of condensate is in line with the seeding hypothesis (note that the opposite was true in the upwind region of seeding with a relative reduction in the rain rates). Though FAD is a useful analysis for seed no-seed comparisons, the Ka-band radar used in Geerts et al. (2010) is more sensitive for smaller cloud drops than the C-band radar used in our study. Some of the small differences here (especially near the surface) are possibly weak-echo attributes and need further research.

Collocated ARG and radar rainfall. The rain rate data from the ARG are taken from the 10×10 km^2 region in the downwind sector (based on the radar Doppler winds) of the seeded location. This analysis relies on the availability of ARGs within this region (details of the method for selecting the ARGs in the sector are provided in Supplement B4). Radar data are taken at every 3×3 km^2 area with ARG location at the center for this analysis. The radar rainfall is calculated using the Marshall–Palmer relationship, $Z = 200R^{1.6}$. The calculated rainfall is again bias corrected.

Ten minutes of rainfall are accumulated every 2 h for each ARG and for each randomized sample. ARG observations were available in the downwind sector for 104 seed and 91 no-seed samples. The average rain rate over 2 h for each randomized case is calculated from the available ARGs in the downwind region of 100 km^2. However, ARG data were available with 44 seed and 42 no-seed samples in this region. The mean rainfall per 2 h per sample is 0.5 ± 1.57 mm for seed samples and 0.36 ± 1.7 mm for no-seed samples. Similarly, the respective mean rainfall over 2 h from radar (at ARG locations) for the seed sample is 0.63 ± 0.99 mm, and for the no-seed sample, 0.51 ± 1.14 mm. Accumulated rainfall over 2 h for 44 seed and 42 no-seed randomized samples are 22.2 and 15.2 mm in the case of ARG, and for radar, the respective values of seed and no-seed are 27.85 and 21.54 mm. The relative enhancement of rainfall with ARG is 46.05% and with collocated radar is 29.29%.

Significance tests. ARG (as per Supplement B4) and radar (data from a 3 × 3 km^2 area around ARG location) rainfall observations in the 100 km^2 downwind region of seeding are used to evaluate the potential seeding effect. The rainfall data obtained from ARG for seed and no-seed conditions were analyzed using two statistical tests, namely, the T2 test and the Mann–Whitney *U* test, to determine the significance of differences between the rainfall populations. The Mann–Whitney *U* test (T2 test) indicated that the mean values of the seeded and nonseeded rainfall populations from ARG were significantly different, with a confidence level above 95% (31%). The relative increase in rainfall for the seeded condition compared to the nonseeded condition was 46%. The uncertainty levels of these two rainfall populations were estimated using MC simulations with 10,000 iterations, considering a 10% increase in standard deviation around their respective mean values. This analysis resulted in an uncertainty of ±13% for the relative increment of 46%.

Radar data were selected for available ARG data locations, and statistical tests were carried out for significant differences between mean values of seed and no-seed rainfall populations. Both tests indicated that their mean values are not significantly different above a 95% confidence level. A relative enhancement of 29% in seeding rainfall is found concerning the no-seeding rainfall in the case of radar. The Monte Carlo simulation, as described above, indicated an uncertainty of ±5% to the relative enhancement of 29%. An additional analysis was done by taking random samples from the no-seed samples alone, and their statistics are checked with MC simulations. Out of 10,000 simulated populations, less than 7% of no-seed and no-seed datasets were significantly different (above 95% confidence level) at 10%–20% of perturbation.

We have also checked the mean values with the bootstrapping method, described in Supplement D2, by generating an ensemble of datasets from the sample dataset, each of seed and no-seed independently, and checking the robustness of the mean values. The analysis showed that the range of the mean values is larger for the seeded cases than the nonseeded cases, both from ARG and radar.

Analysis of radar rainfall over 100 km^2 downwind area. We have extended the analysis for the 100 km^2 downwind area with radar for 150 seed and 122 no-seed samples (note that radar data were not available for one seed and three no-seed samples) from the randomized set, (as mentioned earlier, ARG data were available only for 44 seed and 42 no-seed samples in this region). The average rainfall from radar for every 10-min sample (over 2 h after seeding) is considered for a 100 km^2 area. An investigation with Q–Q plot (Supplement Fig. D4) of the seed and no-seed samples showed that the distribution is skewed for the no-seed dataset with two outliers with very heavy rainfall, indicating the natural rainfall potential over the region. The distribution also showed consistently higher values and was more skewed for seed samples when compared to the no-seed. We introduce a new analysis based on the different percentiles of datasets and respective relative enhancement factors (Fig. 10).

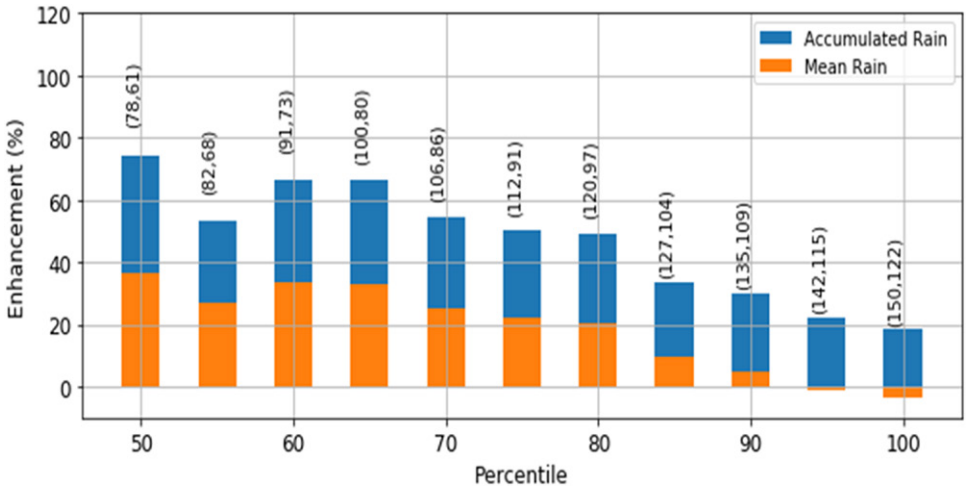

Fig. 10. Relative enhancement factor corresponding to (the mean and accumulated rainfall in the 100 km² area downwind of seeded location) the different percentile of randomized datasets. Numbers given within the parentheses are the number of seed and no-seed (seed, no-seed) samples in each percentile that were used for the relative enhancement estimate.

The analysis showed that 99th percentiles of datasets showed a relative enhancement in the accumulated rainfall, which decreased with an increase in the percentile (as more samples are included in the analysis). The two samples having very high rainfall in the no-seed sample are leading to a decrease in the mean rainfall. We must indicate that the availability of a large number of samples (150 seed and 122 no seed) is a testimony to the rainfall enhancement through hygroscopic seeding with the physical conditions set in CAIPEEX as well as the large uncertainty with the tails of distributions of samples.

Quartile analysis of cloud parameters in its life cycle. We separately considered categories with cloud reflectivity < 30 dB*Z* and > 30 dB*Z* (Figs. 11a,b). The main difference between these two categories is that rain has already developed (>0.2 mm h^{-1}) in the latter case at the start time of seeding. Detailed statistics of this analysis derived from TITAN (Dixon and Wiener 1993) are given in Supplement D3. As seen in the figure, the clouds seeded at an early stage of their development have shown a clear signature of higher reflectivity (especially after 40 min) and longer cloud lifetimes compared to the unseeded clouds. The longer lifetime of seeded clouds is consistent with the seeding hypothesis, and a delay of 20 min is also noted in other reported studies (e.g., Hosari et al. 2021). These clouds gain depth and cross the freezing level, also contributing to forming small hail (graupel) and large drops. Further investigation is required to quantify how many seeded clouds developed ice compared to the unseeded ones. In the no-seed category of clouds, we noted a rapid increase in reflectivity compared to the slow increase in the seed category. Seeded clouds also have lower reflectivity, indicating that drop sizes increase later in the lifetime (nearly 40 min) of the cloud and promote longevity. The seeding in clouds with reflectivity > 30 dB*Z* showed little difference from no-seed clouds. The maximum reflectivity decreases rapidly after 40 (50) min, and there are not many clouds lasting more than 50 (70) min in the no-seed (seed) categories.

Summary of numerical modeling efforts

Numerical models are used as decision support for seeding and to evaluate the physical signature of seeding as we seek linkages between the dynamics and cloud processes to investigate the seeding hypothesis. Adding CCN to warm clouds with low droplet number concentration may develop more LWC and enhance cloud depth and rain rates (Yuan et al. 2011). Warm rain processes are suppressed, and the ice and mixed phase may take a larger role while aerosol is enhanced (Tao et al. 2012; Fan et al. 2013). The tail of the seed particle

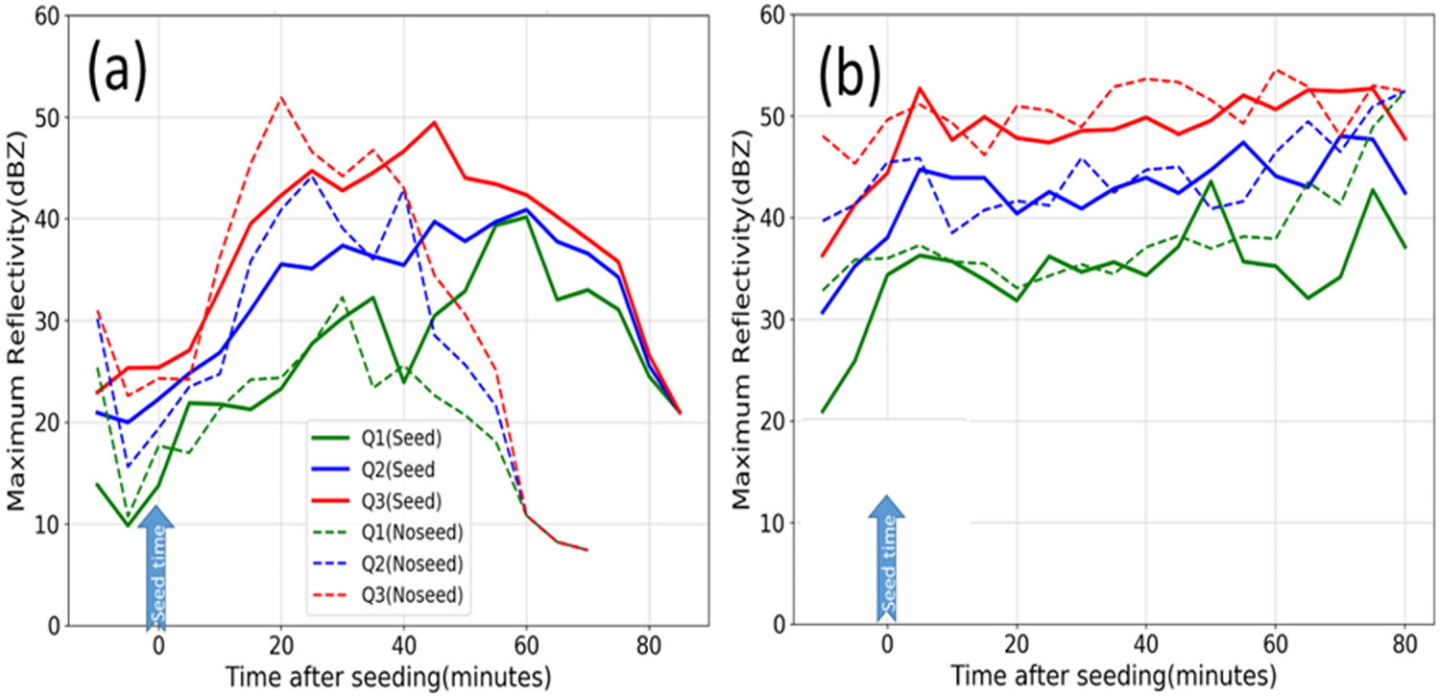

Fig. 11. Time plots of seeded (solid lines) and unseeded (dashed lines) cases with initial maximum reflectivities of (a) <30 and (b) >30 dBZ. All isolated storm histories are delineated into three quartiles (Q1, Q2, and Q3), corresponding to 25%, 50%, and 75% greater than the case value. Time 0 indicates the start time of seeding. More statistics of this analysis and related relative enhancement in various parameters are given in Supplement D3.

size distribution (due to coarse particles) and competition effects (due to small and numerous CCN) are identified (Segal et al. 2004, 2007). The seed particles with larger average sizes than the background aerosols support the tail effect (broadening of DSDs), leading to more rapid precipitation and reducing precipitation efficiency (Konwar et al. 2023). Hygroscopic seeding impacts using direct numerical simulations (DNS) and a hybrid parcel model and the role of the ripening effect and low updraft favoring diffusion growth are documented in other studies (Chen et al. 2020, 2021; Geresdi et al. 2021). The enhanced supersaturation is available due to strong updrafts for activating cloud droplets; the formation of small cloud droplets and the seed particles within clouds can be attributed to the competition effect (Gayatri et al. 2023).

Competition effect. A numerical investigation of hygroscopic seeding with the WRF-LES (Skamarock et al. 2008) model with the same setup as in Gayatri et al. (2022) investigated key microphysical process rates in different stages of convective cloud with and without seeding (Fig. 12) using bin microphysics (Khain et al. 2004; Khain 2009). The key points from the simulation (illustrated in Fig. 12) are 1) threefold enhancement of supercooled liquid (cloud + rain) water, snow, and graupel water content and 2) more rainwater content in the warm region due to a quick rainout in the no-seed case and a delayed enhancement of rain in the seeded case, corroborating the observed findings (Fig. 11). Our findings are also in line with Tonttila et al. (2022), who report that the enhancement in rainfall was 20%–30% in the numerical studies with hygroscopic seeding over the UAE, where the major contribution of rain came from mixed-phase processes, especially due to an enhancement of 15% in the riming rates. Our investigation of process rates showed a significant enhancement in the riming rates, aggregation, freezing, and melting rates (Fig. 12). This demands an advanced understanding of more uncertain processes, such as mixed-phase and secondary ice production processes in the numerical models; however, more field and laboratory studies are needed with focused investigations on the topic to draw solid conclusions.

The numerical investigation suggests that in hygroscopic seeding with flares, delayed growth and suppression of collisions and the presence of drizzle above the freezing level create seeds for graupel by freezing drops; the presence of supercooled water increases deposition, aggregation, riming, and melting rates and enhances subsequent precipitation. The evaporation rates in the cold region of cloud is a detrimental aspect of rainfall.

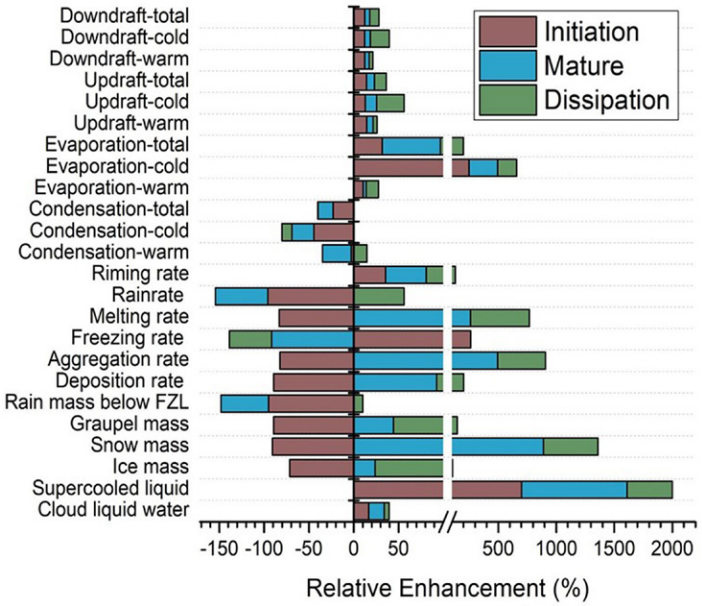

Fig. 12. Relative enhancement [(seed – no seed)/no seed × 100] in the hydrometeor mass and microphysical process rates for three stages of convective cloud (stage I: initiation; stage II: establishing; stage III: mature) from large-eddy simulations of seed and no-seed cases; illustrated is the chain of events in the seeding hypothesis (higher supercooled liquid, snow, and graupel mass, depositional growth of ice particles, condensational heating, freezing, ice aggregation, riming and melting rates, updrafts, and downdrafts). Evaporation rates are also high in the cold region of the cloud, reducing precipitation efficiency. Note that an axis break is introduced at 100% to show all data.

Extra area effects of seeding. The extra area effects refer to the impact of seeding in areas other than the target. The bin microphysics simulations, using the background and flare aerosol size distributions in the WRF Model at 1 km resolution with bin microphysics (Gayatri et al. 2023), provide an example of a physical evaluation with a numerical model combined with observations. The extra area effects of seeding 1) by the seed plume advection downwind in the LLJ and 2) further impact on clouds and precipitation in the downwind area are illustrated. The enhancement factor in the convergence (Banacos and Schultz 2005) of various quantities downwind of the seeded area is illustrated in Fig. 13. The enhancement in CCN at the left corner (longitude of 75°E) of the plot indicates the seeding impact. The rapid enhancement of LWC flux in the seeded plume and a delayed enhancement in the ice water content and rainfall point to the seeding hypothesis, which called for a delayed response to the mixed and ice phase and the rainfall enhancement, is noted 100 km^2 downwind of the seeded area. Results indicate that extra area effects of seeding are also evident in the complete mass transfer downwind of the seeded location. Future work will involve microphysical budgets to quantify these impacts.

The limited explorations of seeding impact with numerical simulations open up new research avenues to reduce uncertainties to be explored with rich datasets and numerical simulations.

Scientific contributions and future work

The CAIPEEX program was initiated in 2009 to investigate the microphysics of monsoon clouds and to address the scientific basis for cloud seeding. The fourth phase of the program was conducted with the recent advances in meteorological instrumentation and cloud seeding methodology based on the WMO recommendations for physical evidence, randomization, and numerical simulations. The physical experiment was executed with two instrumented aircraft for in situ aerosol, cloud, and precipitation measurements, ground-based radar, a suite of aerosol instrumentation, and a dense rain gauge network. A major outcome is the documentation of aerosol–cloud–precipitation interactions, characterizing and tracking

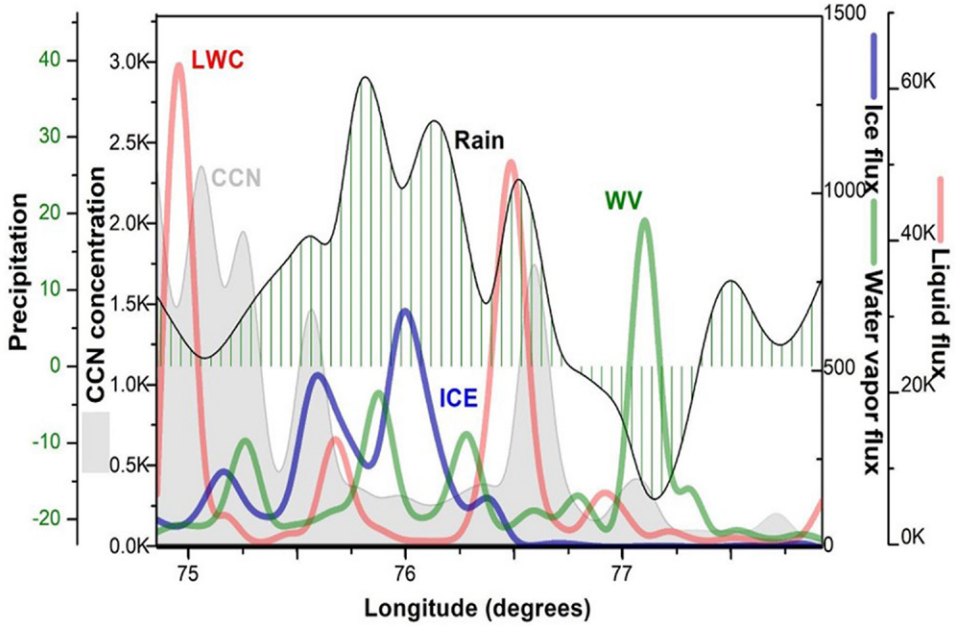

Fig. 13. Relative change (seeded vs control) in the flux convergence of precipitation, liquid water, ice water, and water vapor from the seeding location 75°E to the downwind area (average over 16°–18°N, every 10 km along the longitude).

seed particles in the environment and within clouds, and investigating hygroscopic seeding with randomized experiments and numerical simulations to test the hypothesis that seeding enhances precipitation. The hypothesis called for delayed precipitation and more rainfall, while we must acknowledge that convective clouds have significant uncertainty, attributing to the dry environmental conditions, boundary layer dynamics and inhomogeneities in the aerosol population, warm (liquid)-phase processes affecting the mixed phase, and large-scale monsoon conditions introducing extra area effects of seeding. To summarize:

- Scientific criteria were developed for selecting convective clouds for hygroscopic seeding based on threshold updraft (>1.5 m s^{-1}), cloud liquid water content (>0.5 g m^{-3} at 300 m above the cloud base), and warm cloud layer depth (>1 km). Based on these criteria, 276 randomized samples, 151 (54.7%) seeded and 125 (45.3%) nonseeded, were collected. Overall, the difference between the seed and no-seed samples is significant above a 95% confidence level. Monte Carlo simulations showed a relative enhancement of rainfall with ARG of 46.0% ± 13% and with radar of 29.0% ± 5.0% in the downwind of the seeded location. These results correspond to 31% of randomized samples with collocated ARG and radar observations (from 44 seed and 42 no-seed randomized samples).
- The narrow cloud widths (<10 km), strong downdrafts, and dry environment led to the evaporation of clouds from 83 (55.0%) seed and 86 (68.8%) no-seed randomized samples.
- Radar volume scans of 1,963 clouds in seeded areas and 1,625 in the nonseeded regions show a relative enhancement in rain rates in cloud depth and in the seed areas compared to no-seed. The area-averaged (100 km^{-2}) rainfall in the downwind of seeding from 150 seed and 122 no-seed samples from radar showed a relative enhancement of 18.42% with an uncertainty of ±2.57%. The clouds seeded at an early stage in their development matured more slowly and had a longer lifetime.
- The aircraft conducted more than 5,000 convective cloud penetrations over a 100 × 100 km^2 area throughout the monsoon seasons of 2018 and 2019. The droplet median volume diameter is reduced with a corresponding increase in the droplet number concentration, and large drops or ice particles are generally observed in elevated layers, especially in regions above the freezing level. The number and mass concentrations of

cloud droplets increased in the seed samples compared to those from nonseeded clouds. The presence of numerous small droplets competes for the available water vapor, delaying drizzle formation.
- Advanced aerosol particle spectrometry methods (SP2-XR and a mini-AMS behind a CVI inlet for cloud residuals) were used to identify cloud seeding material within cloud hydrometeor residuals. Identifying seeding signatures in the deep convective cloud volumes up to 4 km has been a key accomplishment of this campaign.
- Numerical simulations using bin and bulk microphysics schemes and flare spectra were used in the model to investigate the extra area effects (Gayatri et al. 2023) and to illustrate the chain of events in seeding hypotheses. The competition effect was investigated from LES and process rates illustrated the seeding hypothesis.

The CAIPEEX experiment yielded one of the highest number of randomized cases with airborne seeding in convective clouds. The UAE research program reported a 23% enhancement (Hosari et al. 2021) in rainfall using the target/control regression with radar observations. The relative enhancement in the cloud duration, precipitating area, and volume was not dramatic (see Supplement D3), as indicated in this UAE study. The approach in CAIPEEX has been unique with airborne seeding in isolated convective clouds and randomization; the seeding location was decided based on the a priori physical basis from previous phases of CAIPEEX and numerical simulations.

The experiment indicates that science-based approaches are mandatory for the effective hygroscopic seeding of convective clouds due to the significant uncertainty associated with natural environmental variability. The ambient environmental conditions before seeding play a crucial role in selecting a suitable time, type, location, and seedability of clouds. The results presented in our study are important for catchment scale projects; however, more caution is to be exercised for aerial cloud seeding operations without proper scientific guidance. Often, operational seeding needs to implement very-high-resolution numerical models to determine the optimal conditions for seeding. Long-term observations and numerical models can provide valuable insight into the windows of opportunity for cloud seeding and assess optimum seeding conditions (Pokharel et al. 2021; Gayatri et al. 2022) over the region.

The experiment has key importance in the arid region, e.g., in Solapur city, where the demand for water supply is 224 million liters per day (MLD), but the average water supply in the city is only 168 MLD. This leads to a demand–supply gap of 56 MLD (84 MLD in peak summer months). The negative impacts of water cycle change on people and ecosystems due to climatic and nonclimatic factors (Douville et al. 2022) are also a grave concern. Global warming and its potential impact on precipitation impose newer challenges for water resources and weather management. The access and exploitation of unconventional water resources (UN-Water 2020; Abshaev et al. 2022), such as cloud seeding, are gaining more interest.

The complex dynamics of convective clouds pose several hurdles, and future studies may require airborne radars and lidars to document the spatiotemporal changes in the physics and dynamics of convective clouds at very high resolution. New technologies, such as unmanned aerial vehicles (Jung et al. 2022; DeFelice et al. 2023; Henneberger et al. 2023), may provide additional avenues for seeding and observations. The importance of convection organization and the impacts of cold pool (CP) developments over the region (Chowdhuri et al. 2021a,b) pose additional challenges with convective cloud seeding and evaluation. Advanced modeling techniques, such as piggybacking (Grabowski 2015; Sarkadi et al. 2022), may be used in future studies to delineate the contribution of convection organization. The representation of fundamental aspects of clouds in models still needs a further understanding of mixed-phase cloud processes and newer approaches to quantify microphysical process rates (Morrison et al. 2020), and future studies will focus on the challenges in understanding and representing them in numerical models.

Acknowledgments. CAIPEEX is fully funded and supported by the Ministry of Earth Sciences (MoES), Govt of India. The Team would like to extend their sincere thanks to Secretary MoES, Director IITM, DG IMD, Head NCMRWF, CAIPEEX National Science Steering Committee members Drs. V. Mudkavi, J. R. Kulkarni, M. M. Sarin, K. Krishnamoorthy, J. P. George, S. Datta, and R. Mehajan. We thank Prof. B. N. Goswami and Late Shri. D. R. Sikka, former Directors of IITM, Dr. A. K Kamra, the IITM family of scientists and administrative staff involved in CAIPEEX in various ways, and Dr. Parvinder Maini, Dr. Gopal Iyengar, Dr. Kamaljit Ray, Dr. R. S. Maheshkumar, at MoES, New Delhi.

We thank technical experts and advisors; Dr. K. Mohankumar, Cochin University of Science and Technology(CUSAT), Dr. V. K, Anandan, Indian Space Research Organization (ISRO), Dr. Thampi and Mr. B. A. M Kannan, India Meteorological Department (IMD) for their support.

IITM established ground-based observational facilities at Savitribai Phule Shikshan Prasarak Mandal's N. B. Navale Sinhgad College of Engineering (SPSPM's NBNSCoE), Solapur, and at Shri Tulja Bhavani College of Engineering (STBCoE), Tuljapur, Maharashtra under Memorandums of Understanding (MoUs). The logistic support from these two colleges and their ongoing support is instrumental in maintaining the ground observational sites at Solapur and Tuljapur. The Team extends special appreciation to Dr. Shankar Dattatray Nawale, the principal of SSPM's NBNSCoE, for his extended support for this project.

The timely support and approvals from the Director General of Civil Aviation (DGCA), Airports Authority of India (AAI), Indian Airforce (IAF), and Airport authorities at Solapur, Pune, Baramati, and Aurangabad, Mumbai, were instrumental in the success of the campaign. We would like to give special thanks to the Pune and Mumbai Air Traffic Controllers (ATC) for being kind in providing necessary aircraft flying permissions throughout the campaign.

We thank Ms. Vishakha C, IITM, for her administrative support throughout the campaign. IITM staff who helped during the field campaign: Dr. Bhupendra Raut, Mr. Imran Syeed (IITM), Mr. Dhananjay Khadge (IITM), Mr. Sunil Kondle, Mr. J Pol (IITM), and others; Mr. Sreekanth Dudhambe (Tesscorn Inc.), Mr. Sachin Patil (Tesscorn Inc.), Mr. Vinayak Ruge (Tesscorn, Inc.) are greatly acknowledged.

The flight plan execution was entirely dependent on our pilots, Mr. Byron and Mr. Nikunj Gandhrokia, sometimes in adverse conditions. Mr. Todd Schulz (WMI, Inc.), Mr. Max (WMI, Inc), and other maintenance engineers, along with the Team of (KCMC LLC), Mr. Prakash Kolliwad, Mr. Srinivas, Mr. Vivek, and other KCMC LLC staff, Dr. Jeff Throckmorton, DMT LLC, all service providers for aircraft operations are acknowledged.

HPC computing at IITM, Pune, and their services were instrumental for the routine model forecasts and simulations presented in the study. Dr. Suryachandra Rao is greatly acknowledged for his timely help with the required HPC resources.

Last, but not least, we are indebted to the Editor, Dr. Manfred Wendisch, and four anonymous reviewers for their time and extensive and constructive comments that helped us to improve the manuscript considerably.

Data availability statement. The datasets on which this paper is based are too large to be retained or publicly archived with available resources. Documentation and methods used to support this study are available from thara@tropmet.res.in at IITM, Pune. IMD high-resolution gridded rainfall data are available at https://www.imdpune.gov.in/cmpg/Griddata/Rainfall_25_Bin.html. Gridded National Centers for Environmental Prediction (NCEP) reanalysis wind data are obtained from https://psl.noaa.gov/data/gridded/data.ncep.reanalysis2.html.

References

Abshaev, A. M., A. Flossmann, S. T. Siems, T. Prabhakaran, Z. Yao, and S. Tessendorf, 2022: Rain enhancement through cloud seeding. *Unconventional Water Resources*, Springer International Publishing, 21–49, https://link.springer.com/10.1007/978-3-030-90146-2_2.

Albrecht, B. A., 1989: Aerosols, cloud microphysics, and fractional cloudiness. *Science*, **245**, 1227–1230, https://doi.org/10.1126/science.245.4923.1227.

American Meteorological Society, 2023: Drizzle. Glossary of Meteorology, https://glossary.ametsoc.org/wiki/Drizzle.

Andreae, M. O., D. Rosenfeld, P. Artaxo, A. A. Costa, G. P. Frank, K. M. Longo, and M. A. F. Silva-Dias, 2004: Smoking rain clouds over the Amazon. *Science*, **303**, 1337–1342, https://doi.org/10.1126/science.1092779.

Banacos, P. C., and D. M. Schultz, 2005: The use of moisture flux convergence in forecasting convective initiation: Historical and operational perspectives. *Wea. Forecasting*, **20**, 351–366, https://doi.org/10.1175/WAF858.1.

Chen, S., L. Xue, and M.-K. Yau, 2020: Impact of aerosols and turbulence on cloud droplet growth: An in-cloud seeding case study using a parcel–DNS (direct numerical simulation) approach. *Atmos. Chem. Phys.*, **20**, 10111–10124, https://doi.org/10.5194/acp-20-10111-2020.

——, ——, and M. K. Yau, 2021: Hygroscopic seeding effects of giant aerosol particles simulated by the Lagrangian-particle-based direct numerical simulation. *Geophys. Res. Lett.*, **48**, e2021GL094621, https://doi.org/10.1029/2021GL094621.

Chowdhuri, S., K. Todekar, P. Murugavel, A. Karipot, and T. V. Prabha, 2021a: Unravelling the turbulent structures of temperature variations during a gust front event: A case study. *Environ. Fluid Mech.*, **21**, 263–281, https://doi.org/10.1007/s10652-020-09769-z.

——, ——, and T. V. Prabha, 2021b: The characterization of turbulent heat and moisture transport during a gust-front event over the Indian Peninsula. *Environ. Fluid Mech.*, **21**, 907–924, https://doi.org/10.1007/s10652-021-09802-9.

DeFelice, T. P., and Coauthors, 2023: Modern and prospective technologies for weather modification activities: A first demonstration of integrating autonomous uncrewed aircraft systems. *Atmos. Res.*, **290**, 106788, https://doi.org/10.1016/j.atmosres.2023.106788.

Dixon, M., and G. Wiener, 1993: TITAN: Thunderstorm Identification, Tracking, Analysis, and Nowcasting—A radar-based methodology. *J. Atmos. Oceanic Technol.*, **10**, 785–797, https://doi.org/10.1175/1520-0426(1993)010<0785:TTITAA>2.0.CO;2.

Douville, H., and Coauthors, 2022: Water remains a blind spot in climate change policies. *PLOS Water*, **1**, e0000058, https://doi.org/10.1371/journal.pwat.0000058.

Fan, J., L. R. Leung, D. Rosenfeld, Q. Chen, Z. Li, J. Zhang, and H. Yan, 2013: Microphysical effects determine macrophysical response for aerosol impacts on deep convective clouds. *Proc. Natl. Acad. Sci. USA*, **110**, E4581–E4590, https://doi.org/10.1073/pnas.1316830110.

Flossmann, A. I., M. Manton, A. Abshaev, R. Bruintjes, M. Murakami, T. Prabhakaran, and Z. Yao, 2018: Peer review report on global precipitation enhancement activities. WWRP-2018-1, World Weather Program, 118 pp., https://community.wmo.int/en/wwrp-publications.

——, ——, ——, ——, ——, ——, and ——, 2019: Review of advances in precipitation enhancement research. *Bull. Amer. Meteor. Soc.*, **100**, 1465–1480, https://doi.org/10.1175/BAMS-D-18-0160.1.

Gayatri, K., S. Patade, J. Fan, and T. Prabhakaran, 2022: Pathways of precipitation formation in different thermodynamic and aerosol environments over the Indian Peninsula. *Atmos. Res.*, **266**, 105934, https://doi.org/10.1016/j.atmosres.2021.105934.

——, P. Thara, M. Neelam, K. Mahen, G. Dinesh, B. Shivdas, and P. Murugavel, 2023: Physical evaluation of hygroscopic cloud seeding in convective clouds using in situ observations and numerical simulations during CAIPEEX. *Atmos. Res.*, **284**, 106558, https://doi.org/10.1016/j.atmosres.2022.106558.

Geerts, B., Q. Miao, Y. Yang, R. Rasmussen, and D. Breed, 2010: An airborne profiling radar study of the impact of glaciogenic cloud seeding on snowfall from winter orographic clouds. *J. Atmos. Sci.*, **67**, 3286–3302, https://doi.org/10.1175/2010JAS3496.1.

Geresdi, I., and Coauthors, 2021: Impact of hygroscopic seeding on the initiation of precipitation formation: Results of a hybrid bin microphysics parcel model. *Atmos. Chem. Phys.*, **21**, 16143–16159, https://doi.org/10.5194/acp-21-16143-2021.

Ghate, V., B. Albrecht, P. Kollias, H. Jonsson, and D. Breed, 2007: Cloud seeding as a technique for studying aerosol-cloud interactions in marine stratocumulus. *Geophys. Res. Lett.*, **34**, L14807, https://doi.org/10.1029/2007GL029748.

Goetz, J. D., and Coauthors, 2018: Speciated online PM1 from South Asian combustion sources – Part 1: Fuel-based emission factors and size distributions. *Atmos. Chem. Phys.*, **18**, 14653–14679, https://doi.org/10.5194/acp-18-14653-2018.

Grabowski, W. W., 2015: Untangling microphysical impacts on deep convection applying a novel modelling methodology. *J. Atmos. Sci.*, **72**, 2446–2464, https://doi.org/10.1175/JAS-D-14-0307.1.

Gumber, S., S. Ghosh, S. Bera, and T. V. Prabhakaran, 2022: On the importance of non-ideal sulphate processing of multi-component aerosol haze over urban areas. *Meteor. Atmos. Phys.*, **134**, 37, https://doi.org/10.1007/s00703-022-00877-7.

Henneberger, J., and Coauthors, 2023: Seeding of supercooled low stratus clouds with a UAV to study microphysical ice processes: An introduction to the CLOUDLAB project. *Bull. Amer. Meteor. Soc.*, https://doi.org/10.1175/BAMS-D-22-0178.1.

Hosari, A. T., and Coauthors, 2021: The UAE Cloud Seeding Program: A statistical and physical evaluation. *Atmosphere*, **12**, 1013, https://doi.org/10.3390/atmos12081013.

Houze, R. A., 2012: Orographic effects on precipitating clouds. *Rev. Geophys.*, **50**, RG1001, https://doi.org/10.1029/2011RG000365.

Jung, W., K.-H. Chang, J. W. Cha, J. M. Ku, and C. Lee, 2022: Estimation of available days for a cloud seeding experiment in Korea. *J. Environ. Sci. Int.*, **31**, 117–129, https://doi.org/10.5322/JESI.2022.31.2.117.

Khain, A. P., 2009: Notes on state-of-the-art investigations of aerosol effects on precipitation: A critical review. *Environ. Res. Lett.*, **4**, 015004, https://doi.org/10.1088/1748-9326/4/1/015004.

——, A. Pokrovsky, M. Pinsky, A. Seifert, and V. Phillips, 2004: Simulation of effects of atmospheric aerosols on deep turbulent convective clouds using a spectral microphysics mixed-phase cumulus cloud model. Part I: Model description and possible applications. *J. Atmos. Sci.*, **61**, 2963–2982, https://doi.org/10.1175/JAS-3350.1.

——, V. Prabha, N. Benmoshe, G. Pandithurai, and M. Ovchinnikov, 2013: The mechanism of first raindrops formation in deep convective clouds. *J. Geophys. Res. Atmos.*, **118**, 9123–9140, https://doi.org/10.1002/jgrd.50641.

Konwar, M., R. S. Maheskumar, J. R. Kulkarni, E. Freud, B. N. Goswami, and D. Rosenfeld, 2012: Aerosol control on depth of warm rain in convective clouds. *J. Geophys. Res.*, **117**, D13204, https://doi.org/10.1029/2012JD017585.

——, S. K. Das, S. M. Deshpande, K. Chakravarty, and B. N. Goswami, 2014: Microphysics of clouds and rain over the Western Ghat. *J. Geophys. Res. Atmos.*, **119**, 6140–6159, https://doi.org/10.1002/2014JD021606.

——, N. Malap, A. Hazra, D. Axisa, T. Prabhakaran and A. Khain, 2023: Measurement of flare size distribution and simulation of seeding effect with a spectral bin parcel model. *Pure Appl. Geophys.*, **180**, 3019–3034, https://doi.org/10.1007/s00024-023-03293-z.

Krishnan, R., J. Sanjay, C. Gnanaseelan, M. Mujumdar, A. Kulkarni, and S. Chakraborty, Eds., 2020: *Assessment of Climate Change over the Indian Region.* Springer, 226 pp., https://link.springer.com/10.1007/978-981-15-4327-2.

Kulkarni, J. R., and Coauthors, 2012: The Cloud Aerosol Interaction and Precipitation Enhancement Experiment (CAIPEEX): Overview and preliminary results. *Curr. Sci.*, **102**, 413–425.

——, S. B. Morwal, and N. R. Deshpande, 2019: Rainfall enhancement in Karnataka state cloud seeding program "Varshadhare" 2017. *Atmos. Res.*, **219**, 65–76, https://doi.org/10.1016/j.atmosres.2018.12.020.

Morrison, H., and Coauthors, 2020: Confronting the challenge of modelling cloud and precipitation microphysics. *J. Adv. Model. Earth Syst.*, **12**, e2019MS001689, https://doi.org/10.1029/2019MS001689.

Murty, A. S. R., and Coauthors, 2000: 11-year warm cloud seeding experiment in Maharashtra State, India. *J. Wea. Modif.*, **32**, 10–20.

Nagaraja, K. and Manikiam, B., 2020: Cloud seeding in Karnataka – Initial results. *VayuMandal*, **46** (2), 31–43, https://imetsociety.org/wp-content/pdf/vayumandal/2020462/2020462_7.pdf.

Pai, D., M. Rajeevan, O. Sreejith, B. Mukhopadhyay, and N. Satbha, 2014: Development of a new high spatial resolution (0.25° × 0.25°) long period (1901–2010) daily gridded rainfall data set over India and its comparison with existing data sets over the region. *Mausam*, **65** (1), 1–18, https://doi.org/10.54302/mausam.v65i1.851.

Patade, S., and Coauthors, 2019: Role of liquid phase in the development of ice phase in monsoon clouds: Aircraft observations and numerical simulations. *Atmos. Res.*, **229**, 157–174, https://doi.org/10.1016/j.atmosres.2019.06.022.

Petters, M. D., and S. M. Kreidenweis, 2007: A single parameter representation of hygroscopic growth and cloud condensation nucleus activity. *Atmos. Chem. Phys.*, **7**, 1961–1971, https://doi.org/10.5194/acp-7-1961-2007.

Pokharel, B., and Coauthors, 2021: A modelling examination of cloud seeding conditions under the warmer climate in Utah, USA. *Atmos. Res.*, **248**, 105239, https://doi.org/10.1016/j.atmosres.2020.105239.

Prabha, T. V., A. Khain, R. S. Maheshkumar, G. Pandithurai, J. R. Kulkarni, M. Konwar, and B. N. Goswami, 2011: Microphysics of premonsoon and monsoon clouds as seen from in situ measurements during the Cloud Aerosol Interaction and Precipitation Enhancement Experiment (CAIPEEX). *J. Atmos. Sci.*, **68**, 1882–1901, https://doi.org/10.1175/2011JAS3707.1.

Rosenfeld, D., U. Lohmann, G. B. Raga, C. D. O'Dowd, M. Kulmala, S. Fuzzi, A. Reissell, and M. O. Andreae, 2008: Flood or drought: How do aerosols affect precipitation? *Science*, **321**, 1309–1313, https://doi.org/10.1126/science.1160606.

——, D. Axisa, W. L. Woodley, and R. Lahav, 2010: A quest for effective hygroscopic cloud seeding. *J. Appl. Meteor. Climatol.*, **49**, 1548–1562, https://doi.org/10.1175/2010JAMC2307.1.

Samanta, S., P. Murugavel, D. Gurnule, Y. J. Rao, J. Vivekanandan, and T. V. Prabha, 2021: The life cycle of a stationary cloud cluster during the Indian summer monsoon: A microphysical investigation using polarimetric C-band radar. *Mon. Wea. Rev.*, **149**, 3761–3780, https://doi.org/10.1175/MWR-D-20-0274.1.

Sarkadi, N., and Coauthors, 2022: Microphysical piggybacking in the Weather Research and Forecasting Model. *J. Adv. Model. Earth Syst.*, **14**, e2021MS002890, https://doi.org/10.1029/2021MS002890.

Sarker, R. P., 1966: A dynamical modelling of orographic rainfall. *Mon. Wea. Rev.*, **94**, 555–572, https://doi.org/10.1175/1520-0493(1966)094<0555:ADMOOR>2.3.CO;2.

Segal, Y., A. Khain, M. Pinsky, and D. Rosenfeld, 2004: Effects of hygroscopic seeding on raindrop formation as seen from simulations using a 2000-bin spectral cloud parcel model. *Atmos. Res.*, **71**, 3–34, https://doi.org/10.1016/j.atmosres.2004.03.003.

——, M. Pinsky, and A. Khain, 2007: The role of competition effect in the raindrop formation. *Atmos. Res.*, **83**, 106–118, https://doi.org/10.1016/j.atmosres.2006.03.007.

Skamarock, W. C., and Coauthors, 2008: A description of the Advanced Research WRF version 3. NCAR Tech. Note NCAR/TN-475+STR, 113 pp., https://doi.org/10.5065/D68S4MVH.

Takle, J., and D. S. Pai, 2020: Analysis of summer monsoon rainfall over Maharashtra and its relation with SSTs. *J. Earth Syst. Sci.*, **129**, 122, https://doi.org/10.1007/s12040-020-01388-y.

Tao, W.-K., J.-P. Chen, Z. Li, C. Wang, and C. Zhang, 2012: Impact of aerosols on convective clouds and precipitation. *Rev. Geophys.*, **50**, 2011RG000369, https://doi.org/10.1029/2011RG000369.

Tessendorf, S. A., and Coauthors, 2012: The Queensland Cloud Seeding Research Program. *Bull. Amer. Meteor. Soc.*, **93**, 75–90, https://doi.org/10.1175/BAMS-D-11-00060.1.

——, S. Chen, C. Weeks, R. Bruintjes, R. M. Rasmussen, and L. Xue, 2021: The influence of hygroscopic flare seeding on drop size distribution over southeast Queensland. *J. Geophys. Res. Atmos.*, **126**, e2020JD033771, https://doi.org/10.1029/2020JD033771.

Tonttila, J., A. Korpinen, H. Kokkola, S. Romakkaniemi, C. Fortelius, and H. Korhonen, 2022: Interaction between hygroscopic seeding and mixed-phase microphysics in convective clouds. *J. Appl. Meteor. Climatol.*, **61**, 1533–1547, https://doi.org/10.1175/JAMC-D-21-0183.1.

UN-Water, 2020: UN-Water analytical brief on unconventional water resources. 59 pp., https://www.unwater.org/sites/default/files/app/uploads/2020/08/UN-Water-Analytical-Brief-on-Unconventional-Water-Resources.pdf.

Varghese, M., J. Jose, A. S. Anu, M. Konwar, P. Murugavel, N. Kalarikkal, M. Deshpande, and T. V. Prabha, 2021: Vertical profile of aerosol characteristics including activation over a rain shadow region in India. *Atmos. Environ.*, **262**, 118653, https://doi.org/10.1016/j.atmosenv.2021.118653.

——, N. Malap, M. Konwar, S. Bera, J. Jose, S. P. Bankar, P. Murugavel, and T. V. Prabha, 2023: Impact of monsoon on below cloud base aerosol hygroscopicity over a rain shadow region of India. *Atmos. Res.*, **285**, 106630, https://doi.org/10.1016/j.atmosres.2023.106630.

Werden, B. S., and Coauthors, 2022: Submicron aerosol composition and source contribution across the Kathmandu valley, Nepal, in winter. *ACS Earth Space Chem.*, **7**, 49–68, https://doi.org/10.1021/acsearthspacechem.2c00226.

WMO, 2015: WMO statement on weather modification in 2015. WMO, 14 pp., https://community.wmo.int/en/activity-areas/wwrp/wwrp-working-groups/wwrp-expert-team-weather-modification.

——, 2018: Plans and guidance for weather modification activities. Executive Council: Sixty-ninth session, WMO Rep. WMO-1196, 261–264, https://library.wmo.int/idurl/4/55618.

Xue, L., S. A. Tessendorf, E. Nelson, R. Rasmussen, D. Breed, S. Parkinson, P. Holbrook, and D. Blestrud, 2013: Implementation of a silver iodide cloud-seeding parameterization in WRF. Part II: 3D simulations of actual seeding events and sensitivity tests. *J. Appl. Meteor. Climatol.*, **52**, 1458–1476, https://doi.org/10.1175/JAMC-D-12-0149.1.

——, X. Chu, R. Rasmussen, D. Breed, B. Boe, and B. Geerts, 2014: The dispersion of silver iodide particles from ground-based generators over complex terrain. Part II: WRF large-eddy simulations versus observations. *J. Appl. Meteor. Climatol.*, **53**, 1342–1361, https://doi.org/10.1175/JAMC-D-13-0241.1.

——, ——, ——, ——, and B. Geerts, 2016: A case study of radar observations and WRF LES simulations of the impact of ground-based glaciogenic seeding on orographic clouds and precipitation. Part II: AgI dispersion and seeding signals simulated by WRF. *J. Appl. Meteor. Climatol.*, **55**, 445–464, https://doi.org/10.1175/JAMC-D-15-0115.1.

——, and Coauthors, 2017: WRF large-eddy simulations of chemical tracer deposition and seeding effect over complex terrain from ground- and aircraft-based AgI generators. *Atmos. Res.*, **190**, 89–103, https://doi.org/10.1016/j.atmosres.2017.02.013.

——, S. A. Tessendorf, E. Nelson, R. Rasmussen, D. Breed, S. Parkinson, P. Holbrook, and D. Blestrud, 2022: Comparison between observed and simulated AgI seeding impacts in a well-observed case from the SNOWIE field program. *J. Appl. Meteor. Climatol.*, **61**, 345–367, https://doi.org/10.1175/JAMC-D-21-0103.1.

Yuan, T., L. A. Remer, and H. Yu, 2011: Microphysical, macrophysical and radiative signatures of volcanic aerosols in trade wind cumulus observed by the A-Train. *Atmos. Chem. Phys.*, **11**, 7119–7132, https://doi.org/10.5194/acp-11-7119-2011.

Yuter, S., and R. A. Houze, 1995: Three-dimensional kinematic and microphysical evolution of Florida cumulonimbus. Part II: Frequency distributions of vertical velocity, reflectivity, and differential reflectivity. *Mon. Wea. Rev.*, **123**, 1941–1963, https://doi.org/10.1175/1520-0493(1995)123<1941:TDKAME>2.0.CO;2.